

Fundamental Oscillations of Massive Boson Stars - II

Swarnim Shirke,^{a,1} Bikram Keshari Pradhan^a Debarati Chatterjee^a Laura Sagunski^b Jürgen Schaffner-Bielich^b

^aInter-University Centre for Astronomy and Astrophysics,
Post Bag 4, Ganeshkhind, Pune University Campus, Pune - 411007, India

^bInstitut für Theoretische Physik, Goethe Universität,
Max von Laue Str. 1, 60438 Frankfurt am Main, Germany

E-mail: swarnim@iucaa.in, bikramp@iucaa.in, debarati@iucaa.in,
sagunski@itp.uni-frankfurt.de, schaffner@astro.uni-frankfurt.de

Abstract. Boson Stars (BSs) are macroscopic self-gravitating configurations made of complex scalar fields. These exotic compact objects (ECO) would manifest as dark Boson stars and can contribute to a certain fraction of the dark matter (DM) in the universe. In this work, we study the fundamental non-radial oscillations (f -modes) of massive BSs and the associated gravitational wave (GW) emission. We consider massive scalar BSs having the potential of the form $V(\phi) = \frac{1}{2}m^2|\phi|^2 + \frac{1}{4}\lambda|\phi|^4$, restricting to the strong-coupling regime ($\lambda \gg m^2/M_{Pl}^2$) where solutions resembling fermionic stars are known to exist. We first review the available parameter space for scalar DM that can form massive BSs and enlist various constraints. We fit and provide simple analytical relations connecting various macroscopic observables for BSs, which can be directly incorporated into future studies of massive BSs throughout the strong coupling regime without requiring any numerical computation. We then solve for the non-radial $l = 2$ fundamental quasinormal modes (f -modes) for massive BSs. Scaling relations for f -mode equations have been reported in another work. Using these, we perform a complete study of these oscillations spanning the entire available parameter space of massive BSs and provide analytical fits for the f -mode characteristics. We further study the universal relations for BSs and reveal the parameter space that is sensitive to the current and future planned GW detectors. We find that different parts of the parameters space can, in principle, be probed by the LISA, LIGO, and NEMO detectors. Finally, we briefly discuss the detectability of f -modes from BSs that have not been explored before.

¹Corresponding author.

Contents

1	Introduction	1
2	Model	3
3	Parameter Space	4
3.1	Constraints	4
4	Results	6
4.1	Scaled Relations - I (static observables)	6
4.2	Scaled Relations - II (fundamental modes)	8
4.3	Universal Relations	9
4.3.1	Empirical Fits	10
4.3.2	f -Love- C	11
4.4	Observable parameter space	13
4.5	Detectability	18
5	Discussions	20
5.1	Summary	20
5.2	Comparison with other works	22
5.3	Future Scope	23
A	Scaling of Love equations	24
B	Variation with density	26
C	$\Lambda - M$	26
D	Scaling for Moment of Inertia	27
E	The I-Love-C Relations	28

1 Introduction

Boson stars (BSs) are stellar configurations of bosonic particles (see [1, 2] for updated review on BSs). The formation channels for BSs include primordial density fluctuations in the scalar field, gravothermal collapse in an early matter-dominated era of the universe [3], or a process known as *gravitational cooling* [4]. These are some of the possible exotic compact objects (ECOs) that can mimic other compact objects like black holes (BHs) acting as BH mimickers, as well as contribute to the total DM budget (see [5] for a review on ECOs). When a real scalar field describes these stars, they form a *Soliton star*, also called *Oscillaton* [6]. In these stars, the boson number is not conserved. When the field is complex, the stellar configurations formed thereby are called *Boson Stars* [6], the boson number of which is conserved. When a particle is modelled using vector boson (spin-1), the stars obtained are called *Proca Stars*.

The study of such stars started with the self-gravitating configurations of the electromagnetic field [7]. This was then applied to massive-scale fields by solving the Einstein-Klein-Gordon equations [8–10] and extended later to include self-interactions [11, 12]. Various types of BSs have been studied in the literature. Based on the interaction potential, they are classified into different types of BSs like mini-BS (no interaction), massive BS, axion star, solitonic star, etc. In this work, we will focus on the second type, the massive BSs, which is the simplest form of potential consisting of quartic self-interaction capable of forming massive compact objects as shown in [12].

Being a candidate for dark matter, these particles are assumed to couple sufficiently weakly to electromagnetic (EM) photons and other SM particles. This means that non-accreting BSs are not observable via conventional EM telescopes. This situation is similar to that of black holes (BHs), making them a good candidate for BH mimickers. In the case of accreting systems, the BSs can be distinguished using the EM observations based on the analysis of shadow region [13] and line broadening [14]. These methods are inaccessible in the case of non-accreting BSs. However, the successful detection of gravitational waves [15] has opened up a new window to probe the dark sectors of the universe. There have been many works on this front in the last few decades. These, along with search results so far, have been briefly summarized below.

Head-on collisions of BSs and the associated GW emission were studied in [16–19]. Gravitational echoes from ECOs were explored in [20]. Recently, [21] performed the first simulation of a binary merger of massive BSs and [22] for solitonic stars.

GW190521 was a BBH merger event with at least one of the components having mass lying in the black hole mass gap [23]. There were several beyond standard model (BSM) explanations for explaining this merger [24] along with the possibility of BS mergers [25], in particular, head-on collision of high-spin Proca stars. This was the first instance of the possibility of having detected BS as a BH mimicker through a real GW event, however, later analysis of higher order modes [26] of the ringdown phase ruled out this possibility in favour of BH.

Quasi-normal oscillation modes of stars are important in the context of binary pre- and post-merger as well as isolated system excitations. [27] was the first work to explore the quasinormal modes of BSs. There have been a few studies on BS QNMs following that [28–33]. [31] is the first work to study the f -modes for massive BSs in the strong-interaction limit. However, the work was restricted to stellar mass BSs and select model parameters, as will be discussed later. Another work [33] appeared during the completion of this work that explored BS f -modes for select parameter sets. We report scaling relations in a separate publication [34] and therein compare the BS QNMs with those of BHs and neutron stars (NSs). Spinning BSs are known to form toroidal configurations instead of spherical [35]. We restrict to the non-spinning case in this work.

We extend the work of [31, 33] to make a more general case. As will be discussed, a large parameter space in terms of DM mass and its self-interaction strength λ is available for BSs. In [34], we show for the first time that scaling relations are followed for the f -mode frequency and damping time in the strong-interaction limit. This scaling result is significant, as it allows us to comment on f -mode characteristics of configurations of arbitrary parameters within the strong-interaction limit ($\Lambda_{int} \gg 1$). We provide analytical fits to the static as well as f -mode solutions for massive BSs and also study the universal relations. We estimate the parameter space accessible for existing and future GW detectors and comment on the detectability of BSs using f -modes.

The article is organized as follows: In Sec. 2 we provide the details of the BS model, describing the scaling property of massive BS. We discuss the available scalar DM parameter space in Sec. 3, reviewing all the available constraints. We present all the results in Sec 4, discussing the static observables, f -modes, and the corresponding universal relations. We also comment on the parameter space observable using GW from f -modes from massive BSs and discuss the detectability by various GW detectors. We summarize our results in Sec. 5, providing a comparison with earlier works and outlining the future scope.

We use the convention $\hbar = c = 1$ and hence $G = 1/M_{Pl}^2$ throughout this work.

2 Model

Here, we provide details of the model used to describe Bosonic DM that will be used to study BS f -modes in this work. We also show the scaling relations used.

We describe DM by scalar field self-interacting via quartic self-interactions as elaborated in [12, 31]. The interaction strength is given by λ .

$$\mathcal{L} = \frac{1}{2}\partial_\mu\phi^*\partial^\mu\phi + V(\phi) \quad (2.1)$$

$$V(|\phi|) = \frac{1}{2}m^2|\phi|^2 + \frac{1}{4}\lambda|\phi|^4 \quad (2.2)$$

Here λ is the self-interaction coupling, and m is the mass of the DM particle. A dimensionless parameter is defined as

$$\Lambda = \frac{\lambda M_{Pl}^2}{4\pi m^2}. \quad (2.3)$$

For $\Lambda \gg 1$, [12] showed that we could form massive stars whose mass resembles that of a degenerate fermionic star. In this case, $M_{max} = 0.22\sqrt{\Lambda}M_{Pl}^2/m = 0.06\sqrt{\lambda}M_{pl}^3/m^2$ [12]. The macroscopic properties are dictated by the effective factor defined as [21]

$$x \equiv \sqrt{\lambda/m^2}. \quad (2.4)$$

Using this, we define the dimensionless mass (M') and dimensionless radius (R') as $M' = M/(xM_{Pl}^3)$, $R' = R/(xM_{Pl})$. The dimensionless energy density and pressure are scaled as $\rho' = \rho x^2$, $p' = p x^2$.

We consider here the case of self-interacting massive BSs, for which $\Lambda \gg 1$ and the scalings hold. We restrict our analysis to $\Lambda > 1000$, referred to as the strong-interaction limit [36]. In this limit, the Einstein-Klein-Gordon system of equations for the scalar field resembles that of a perfect fluid star with the effective equation of state given by [12, 21, 37],

$$p' = \frac{1}{9}(\sqrt{1+3\rho'} - 1)^2. \quad (2.5)$$

For $\rho' \ll 1$, $p' = \rho'^2/4$, i.e. we get a polytrope EoS with polytropic index $n = 1$. For $\rho' \gg 1$, we get an ultra-relativistic EoS $p' = \rho'/3$. We will show later that this condition is not reached inside BSs (Appendix. B).

For the f -mode frequencies and damping times, we solve the f -mode eigenfrequencies using full-GR formalism and use the following scaling relations as reported in [34]

$$f = f'/(xM_{Pl}) \quad (2.6)$$

$$\tau = \tau'(xM_{Pl}). \quad (2.7)$$

The formalism and derivation of scaling have been provided in detail in the Appendix of [34].

3 Parameter Space

Fig. 1 shows the available parameter space in the $\lambda - m$ space for scalar DM. For mass, we show the range $10^{-25}\text{eV} < m < 100\text{GeV}$ covering the mass of fuzzy DM or ultralight ALPs to roughly the mass of WIMPs. We consider λ upto $\lambda = 15$. This encompasses the upper limit of $\sim 4\pi$ as imposed by [38]. All the constraints are discussed in detail in the next section. The values $\lambda \lesssim 10^{-100}$ are irrelevant as lower values consistent with observations do not fall in the strong-interaction limit considered here. The yellow lines denote contours of fixed Λ , and this analysis is only applicable to $\Lambda > 1000$, i.e., the strong-interaction regime. The translucent region is the Kaup limit where $\Lambda \ll 1$ and interactions can be ignored. The gray lines show contours where σ/m is constant, and the region between them is the region permitted by other astrophysical observations. We note that this is a very narrow region in the parameter space; however, the lower bound (dashed gray line) is not strict. The red line marks the constraint from CMB and LSS data [39]. The region above this line is excluded. The blue region is excluded by the recently set lower limit in scalar DM mass [40] using dwarf galaxies.

The maximum mass of the Bosonic dark star is shown in colour. This can be calculated for a given set of parameters (λ, m) is given by [12]: $M_{max} = 0.22\sqrt{\Lambda}\frac{M_{Pl}^2}{m} = 0.06\frac{\sqrt{\Lambda}}{m^2}M_{Pl}^3 = 0.06xM_{Pl}^3$. The colour scale saturates into yellow at $M_{max} = 20^{22}M_{\odot}$, which is the rough estimate for the universe's mass. We plot the contours of some fixed mass values. We find that the M_{max} ranges a larger region in mass spanning mountain mass to galactic mass (see. caption of Fig. 1). The arrows indicate the regions allowed by various constraints. The only region bounded by the gray (σ/m), red (CMB, LSS), and blue (dwarf galaxies) lines is the allowed region for scalar DM and, hence, BSs. Further, this work is only applicable in the region bounded by the yellow (strong-interaction regime) line, i.e., the strong interaction regime.

Flores et al. [31] restricted their study to stellar mass BSs and used selected values of $m \in \{1, 1.25, 1.5, 1.75, 2\}m_n$ and $a \in \{5, 10, 15, 20\}$ fm to study the f -modes. The scattering length parameter $a = \lambda/8\pi m$ was used to fix interaction strength instead of λ in [31]. These are marked by a purple patch in Fig. 1. Maselli et al. [41] studied the I -Love- Q relations using a select set of model values. The parameters chosen were $m \in \{300, 400\}$ MeV and $\lambda \in \{0, 0.5, 1.5\}\pi$. Celato et al. [33] explored the f -mode universal relations for the same parameters. These are marked in orange in Fig. 1. It is clear that both these patches lie near the $M_{max} \sim 1M_{\odot}$ contour and focus on the configurations in the NS mass range.

3.1 Constraints

Cross-section: The interaction cross-section between the DM particles for this model is given by [38]

$$\sigma = \frac{\lambda^2}{64\pi m^2} . \quad (3.1)$$

The small-scale problems in the Λ CDM model and cold DM-only simulations like the i) cusp-core problem, ii) missing satellite problem, iii) too big to fail problem are known to be resolved by allowing for self-interacting DM (SIDM) [42]. These studies demand that the interaction strength be satisfied to a particular range in order to resolve the problems. The bounds on σ/m are given by $0.1 < \sigma/m < 100 \text{ cm}^2/\text{g}$. The upper limit is usually known to be around $10\text{cm}^2/\text{g}$, however we consider here least constraining case allowing for more

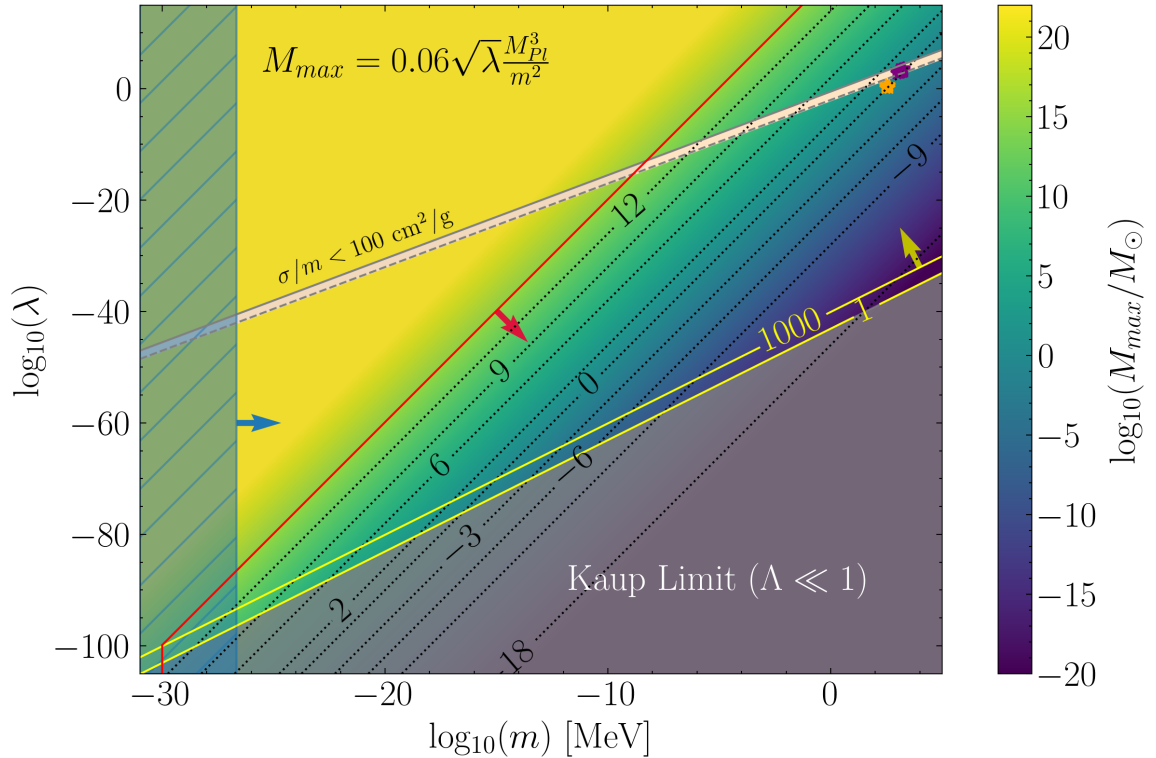


Figure 1. Figure shows the available parameter space in the $\lambda - m$ space. The color indicates the logarithm of the maximum mass of a stable BS for a given pair of (λ, m) . We show select contour lines (black) to get an idea of masses: $\log_{10} M = -18$ (mountain mass; this is also the lower bound on primordial BH set by Hawking radiation as lighter PBHs would evaporate within Hubble time); -9 (asteroid belt mass); -6 (Earth-like planet mass); -3 (giant planet mass); 0 (stellar mass); 2 (giant massive star mass); 6 and 9 (SMBH mass); 12 (galaxy mass). The red line gives an upper limit λ and a lower limit on m from CMB and LSS data [39]. The blue line marks the lower limit on scalar DM mass [40] from dwarf galaxies. The yellow contours represent values of Λ . We restrict to the strong-interaction limit $\Lambda > 1000$ in this work. $\Lambda \ll 1$ is the non-interacting/Kaup limit shaded in gray. The bisque band is the from the bounds on σ/m . The upper limit and lower limit are marked by a solid and dashed line, respectively. The lower bound is not strict. See text for details. The purple patch denotes the parameters used in [31] to study f -modes of massive BS. The orange patch indicates the parameters used by [33, 41] to study the I -Love- Q and f -mode universal relations.

flexibility and the largest possible parameter space. Thus,

$$0.1 < \frac{\lambda^2}{64\pi m^3} < 100 \text{ [cm}^2/\text{g]} \quad (3.2)$$

The upper limits come primarily from observations of merging clusters (for e.g., Bullet Cluster), whereas the lower bounds arise from the assumption that self-interactions alone are responsible for the resolution of the aforementioned problems encountered in CDM-only simulations (see [42] for a comprehensive list of all constraints). There are alternative solutions to these problems, the most obvious one being the inclusion of baryonic feedback at small scales. Thus, the lower bound is not strict, and hence, we denote it by a dashed line in Fig. 1. Only parameters consistent with these constraints were considered in [31]. However, we see a large range of parameter space is allowed, and stellar mass BSs can be produced even when

the lower bound is removed.

Seoane et al. [36] added constraints on the parameters space, assuming the object at the centre of our Milky Way is a BS (acting as a BH mimicker). This gave $3.4^4 \leq m/\lambda^4 \leq 2.9 \times 10^5$ [eV]. A similar analysis for NGC 4258 gave $6.3 \times 10^4 \leq m/\lambda^4 \leq 9.6 \times 10^5$ [eV]. However, we do not make such an assumption while exploring the parameter space. Also, it is now established that Sagittarius A* is an SMBH [43], which is also true for the M87 galactic centre [44]. Arbey et al. [45] fitted scalar DM to galaxy rotation curves of dwarf spiral galaxies and obtained $50 < m^4/\lambda < 75$ [eV⁴]. This corresponds to M_{max} of $\mathcal{O}(10^{16})$, which is too large to be considered for our study of compact BSs. Eby et al. [38] impose the constraint of $\lambda \lesssim 4\pi$ for perturbative reasons, which, when combined with σ/m constraint, allow DM of mass of only below 100 MeV approximately. We do not consider this condition here.

Mass: Fuzzy DM can be described by ultra-light ALPs roughly in the mass range $m \in [10^{-25}, 10^{-17}]$ eV. Planck Collaboration put a lower bound on the DM mass of fuzzy DM as $m \gtrsim 10^{-25}$ eV using the CMB anisotropies. This has been updated to $m \gtrsim 10^{-23}$ eV by combining these results with Dark Energy Survey- Year 1 data [46] for weak gravitational lensing and to $m \gtrsim 2 \times 10^{-20}$ eV using the Lyman-alpha forest [47]. More bounds were added from the study of the number of satellite galaxies for Milky Way as $m \gtrsim 2.9 \times 10^{-21}$ eV [48] and $m \gtrsim 2.5 \times 10^{-22}$ eV from the study of UV luminosities of high-redshift galaxies using Hubble and James-Webb telescopes [49]. These bounds on Bosonic DM assume axion potentials, which mimic massive BS potential for weak coupling.

For the quartic potential case, [39] derived a lower bound of $m \gtrsim 10^{-24}$ eV using CMB and large-scale structure data of Planck Collaboration [50] and WiggleZ Dark Energy Survey [51]. There is a corresponding upper bound on λ given as $\lambda/m^4 < 10^{20.14}$ [MeV⁻⁴]. This corresponds to $M_{max} \sim \mathcal{O}(10^{15})M_\odot$, which is much larger than the masses we are interested in for BSs. We still show it by a red line in Fig. 1. This also corresponds to an upper bound in x given by $x < 10^{10.07}$. These constraints were used to study the admixture of Bosonic DM in NS in [52].

The bounds discussed so far are model-dependent. Recently, Zimmerman et al. [40] derived a robust bound of $m \gtrsim 2.2 \times 10^{-21}$ eV using dwarf galaxies, which does not depend on the assumed cosmology, microphysics, or dynamics of dark matter. The only assumption is that the DM is composed of a single scalar degree of freedom. This bound is shown in Fig. 1 as a blue-hatched exclusion region.

The recent discovery of stochastic GW background by the International Pulsar Timing Array (IPTA) also opened up a way to probe ultralight DM (ULDM). The array is sensitive to DM in the mass range $10^{-24} \lesssim m \lesssim 10^{-20}$ eV. The NANOGrav collaboration found no significant evidence for ULDM in the range $10^{-24} \lesssim m \lesssim 10^{-20}$ eV, while the EPTA collaboration concluded that ULDM in the mass range $10^{-24} \lesssim m \lesssim 10^{-22.3}$ eV cannot alone explain the DM budget. The bound by [40] is still higher than these, so we do not consider these.

4 Results

4.1 Scaled Relations - I (static observables)

We first discuss the scaling of the mass-radius relations along with compactness. This scaling property in the strong-interaction limit was first shown by Colpi et al. [12]. The self-similarity of the Tolman-Oppenheimer-Volkoff (TOV) equations was shown in [41]. In terms of the scaled quantities, the maximum mass observed is $M'_{max} = 0.06$, and the maximum compactness is

$C_{max} = 0.16$. For BSs, we can, in principle, go arbitrarily low in mass and compactness. In such a case, the radius reached a saturation value of $R'_{max} = 0.625$.

We derive analytical fit relations for the scaled $M' - C$, $R' - C$, and $M' - R'$ curves obtained by solving the scaled TOV equation (see Appendix of [41]), which we did not find in any previous literature. A recent work [53] provided fits for specific regions of the mass curve of mini-BSs (Kaup limit). Fit relations would enable switching between the quantities M , R , and C using simple analytic expressions. Compactness is the most natural control variable for BSs as it does not scale with model parameter x . For this reason, we provide analytical fits for all quantities in terms of compactness wherever feasible.

In Fig.2(a), we plot the scaled mass M' as a function of compactness C . M' increases with C from (0,0) and reaches a values of $M'_{max} \approx 0.06$ at $C'_{max} \approx 0.16$. We perform fitting only up to this critical point as the region after it, where the mass decreases, is unstable and not of interest. We fit quadratic and quartic functions of the form

$$\begin{aligned} Y &= a_0 + a_1X + a_2X^2 , \\ Y &= b_0 + b_1X + b_2X^2 + b_3X^3 + b_4X^4 . \end{aligned} \quad (4.1)$$

For this fit, we take $Y = M'$ and $X = C$. The fit coefficients are given in Table. 1. We solve for f -modes for a minimum compactness of 0.02 in this work, so we restrict ourselves to $C \gtrsim 0.02$. This is lower than the minimum compactness of $C = 0.035$ considered in previous works [54, 55]. For $C \gtrsim 0.02$, we observe that the quadratic functions provide a good fit with an accuracy within 2%. For the case of quartic fit, the accuracy is within 0.25%. Using the fit for $M' - C$, we get $M'(C = 0.02) \approx 0.012$. So, in this work, we focus on BS configurations with $M' \gtrsim 0.012$.

We also plot the relation given in Eq. A2 of [56] (see Eq. C.1) in yellow. This fit was derived for zero spin while studying the variation of C^{-1} for different mass configurations as a function of dimensionless spin $\chi = J/M^2$, where J is the spin angular momentum of BS. From the plot, we see that this does not fit the $M - C$ curve for non-rotating BS. This also results in a departure from expected values of k_2 (see Fig. 6 of [56]) as shown in Fig.B. Thus, our fit provides a new analytical relation for the same.

Next, we fit the scaled radius as a function of compactness, i.e., $Y = R'$, $X = C$. We show the dependence in Fig. 2(b). As we increase the compactness, the radius decreases. The scaled radius decreases from $R' = 0.6$ for $C = 0.02$ down to a minimum value of $R'_{min} = 0.38$. We show the quadratic and quartic fits as described in Eqn. 4.1 in blue and green, respectively. The accuracy is sub percent level, with that of the quadratic fit being under 1% and that of the quartic fit being under 0.1% for $C \gtrsim 0.02$. The fit coefficients are reported in Table. 1.

We show the well-known $M' - R'$ curve in Fig.2(c). Here $Y = M'$, $X = R'$. At low, masses ($M' \rightarrow 0$), the radius reaches a constant values of $R'_{max} = 0.626$. R' decreases as M' increases and reaches a minimum value of $R' = 0.38$ as M' reaches a maximum value of $M' = 0.06$. We perform fits using the same functions as given in 4.1 with $y = M'/M'_{max} = M/M_{max}$ and $x = R'/R'_{max} = R/R_{max}$. The fit coefficients are given in Table. 1. So below $R'(C = 0.02) = 0.6$, the quadratic function fits within an accuracy of 3.5%, and the quartic function within 0.75%.

The dimensionless tidal deformability (Λ) does not scale with x . This has been derived in Appendix A. We show how the quantities above (M, R, C) vary with the central density in Appendix. B. We show the $\Lambda - M'$ solution in Appendix. C and compare it with the previous results so far. The scaling for the moment of inertia has been derived in Appendix. D.

Y	X	a_0	a_1	a_2	b_0	b_1	b_2	b_3	b_4
M'	C'	-3.545×10^{-4}	0.665	-1.705	-3.191×10^{-5}	0.634	-1.466	3.142	-23.295
R'	C'	0.626	-1.044	-2.784	0.626	-1.061	-4.256	31.617	-141.821
M'	R'	-0.119	0.910	-1.150	-0.254	2.234	-5.814	7.042	-3.866

Table 1. Fitting coefficients for the quadratic and quartic function fits to $M - C$, $M - R$, and $R - C$ as given in Eqs. 4.1. These coefficients are used to plot the fitting functions in Figs. 4.1 and 4.1.

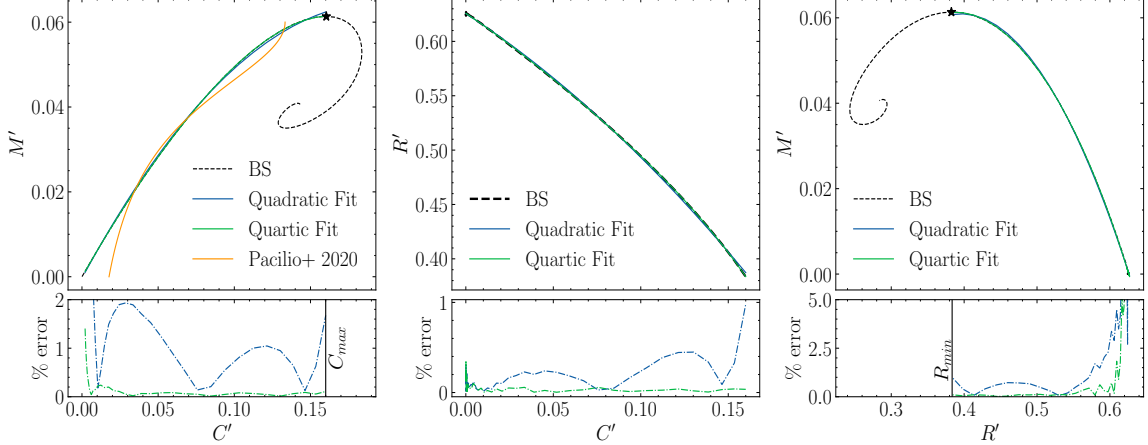


Figure 2. Quadratic (blue) and quartic fits (green) for (a) $M' - C'$, (b) $R' - C'$, and (c) $M' - R'$ relations for massive BSs in the strong-interaction limit. The dashed black line is the actual calculated numerical solution. The yellow curve is taken from [56], where the fit is derived for non-spinning massive BS. The percent errors for both fits are shown in the lower panels of each figure. The star marks the point beyond which the BS configurations become unstable. The stable solutions are valid only for compactness (radius) below (above) the star.

4.2 Scaled Relations - II (fundamental modes)

We now move to f -modes, which is the focus of our work. We showed in [34] that upon applying the scaling $f' = fxM_{Pl}$ and $\tau' = \tau/xM_{Pl}$, we get unique solutions for f -mode characteristics as a function of M' and C . This is because the f -mode equations and perturbation equations are completely independent of model parameters when written in scaled coordinates. We have shown this explicitly in the Appendix of our other work [34]. We can use then scaling to obtain the $f - M$ curve for any set of (λ, m) parameters.

We show this curve as obtained in [34] in Fig. 3(a) with a black-dashed line. f' increases with M' and reaches a maximum value of $f'_{max} = 0.21$ for the maximum mass configuration of BS. We observe that the curve begins with a constant slope at low mass, and the slope diverges as it reaches the maximum mass. Hence, we fit a hyperbola to this relation given by

$$f' = -7.297 \sqrt{\left(\frac{M' - M'_{max} - 189.0116}{189.0116}\right)^2 - 1} + f'_{max}. \quad (4.2)$$

Here we have imposed the condition that $f'(M' = M_{max}) = f'_{max}$. The error of this fit is shown in the lower panel of Fig. 3(a). This fit agrees with the numerical solution within 3%. We also show the solution for $f' - C'$ in Fig. 3(b) as compactness is a more natural variable. This, too, is an increasing function, and we fit the quadratic and quartic functions

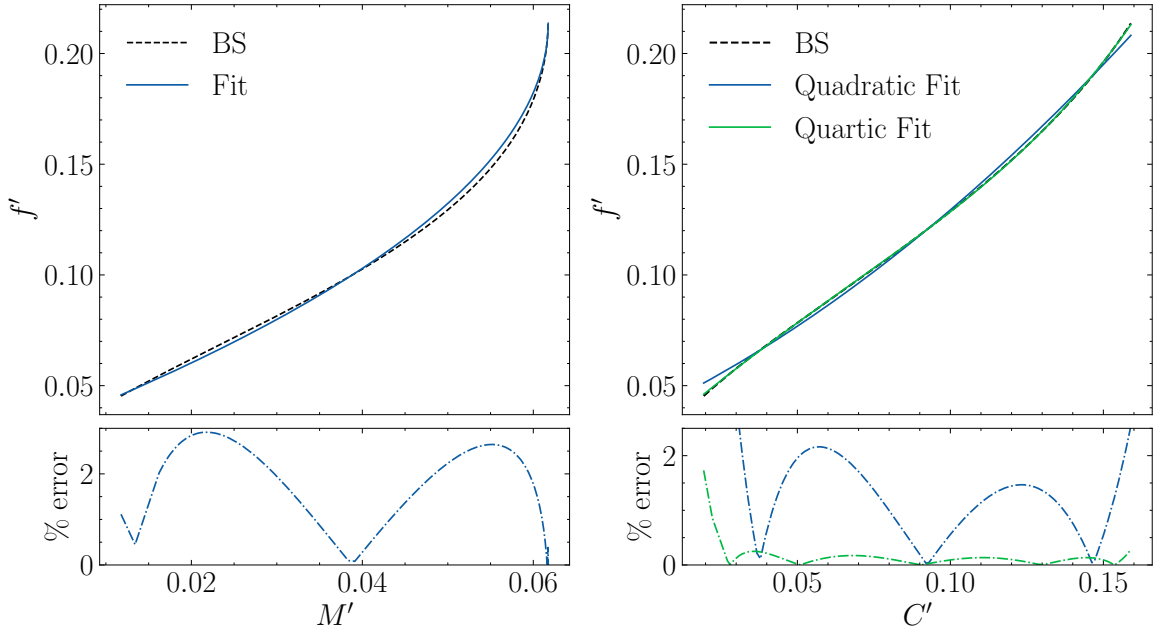


Figure 3. The scaled dimensionless f -mode frequency (f') as a function of a) scaled mass of BSs and b) compactness. The blue curve in the left panel is the fitted hyperbola as given in Eq. 4.2. The blue and the green curves in the right panel are the fits for the quadratic and quartic functions, respectively, as given in Eqn. 4.1. The fit coefficients are given in Table. 2. The lower panel shows the percent error for each fit.

Y	X	a_0	a_1	a_2	b_0	b_1	b_2	b_3	b_4
f'	C'	3.747×10^{-2}	0.656	2.627	2.363×10^{-2}	1.203	-2.232	-4.417	113.160
M'	$1/\log \tau'$	—	—	—	-9.718×10^{-2}	4.457	-84.357	7.771×10^2	-2.460×10^3
τ'	$1/C'$	—	—	—	4.124×10^2	-1.147×10^2	24.602	5.030	3.856×10^{-3}

Table 2. Fitting coefficients for the fits between the quantities f' , τ' , M' , and C' as given in Eqs. 4.1. The fit for $f' - M'$ is given in Eq. 4.2.

given in Eqn. 4.1. Here $Y = f'$ and $X = C$. The quadratic fit diverges for both low and high compactness. The quartic fit is accurate to 1% for $C \gtrsim 0.02$. The fit coefficients are reported in Table. 2.

Next, we show τ' as a function of M' and C' as reported in [34] in Fig. 4. τ' is decreasing function of M' and C as expected. We use the log scale for τ' as it varies by orders of magnitude. The minimum value of τ' corresponding to the maximum mass configuration is $\tau'_{min} = 1900$ [34]. This single fit is sufficient to reproduce all the results and for the entire parameter space in the strong coupling regime ($\Lambda \gg 1$) using scaling relations.

For both cases, we fit the quartic polynomial of the form Eq. 4.1. For the $\tau' - M'$ fit we use $X = 1/(\log \tau')$ and $Y = M'$ as in the case of $\Lambda - M'$ relation [56, 57]. We find the error is within 5%. For the case of $\tau' - C'$, choose $X = 1/C'$ and $Y = \tau'$. The fit has a percent level of accuracy. The fit coefficients are provided in Table. 2.

4.3 Universal Relations

In this section, we discuss some known universal relations and fitting functions, focusing on the f -mode characteristics. The other known relations for static stars, in particular the I -

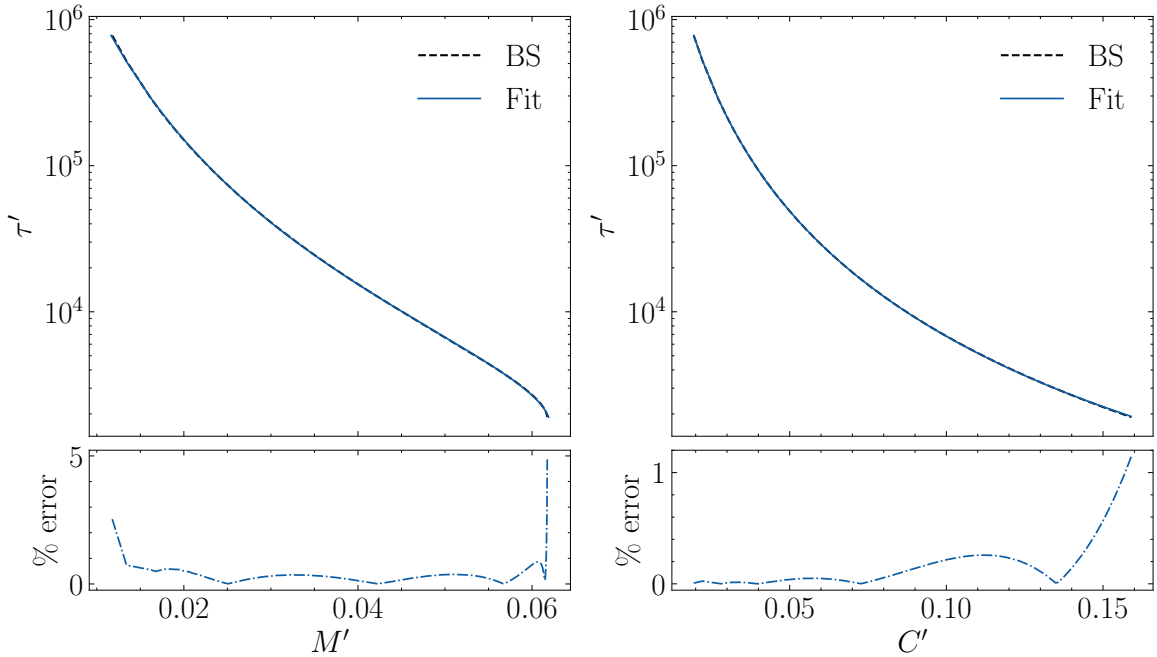


Figure 4. Same as Fig. 3 but for the scaled dimensionless f -mode damping time (τ').

Love- C , are discussed in Appendix. E. Here, we use the scaling derived in Appendix. A and Appendix. D to show the I –Love– C universal relations are exact for massive BSs. Compact stars are known to follow some empirically observed universal relations, which can be used to infer stellar properties from observations of stellar observations. Such inference of stellar properties using observation of pulsations comes under the study of asteroseismology. Here, we would like to connect the macroscopic properties of BSs to its fundamental non-radial QNM, f -modes.

4.3.1 Empirical Fits

The f -mode frequency is known to scale with the square root of average density (M/R^3) of NS and was first proposed by [58, 59]. The relation is of the form

$$f(\text{kHz}) = a + b\sqrt{\frac{GM}{R^3}}. \quad (4.3)$$

Here, f is the f -mode frequency, M is the mass of the star, and R is its radius. a and b are the fitting coefficients.

This relation holds for ordinary NSs [59, 60], for NSs with hyperons [61], and also for DM admixed NS [62] as shown recently using the neutron decay model for DM. This relation was also checked for BSs for select values of λ and m in [31] that form BSs with masses in the range of NSs. The fit was performed for each set individually. The coefficients reported considering all the sets were $a = -0.0195 \pm 0.0008$ kHz and $b = 62.997 \pm 0.058$ kHz km. The relation was also explored in [33] for select BS cases and reported the coefficients $a = -0.01461$ kHz and $b = 42.11$ kHz km. Also, to compare with the coefficients for other NS cases, a is known to lie within the range 0.22 – 0.79 kHz and b within 32 – 48 kHz km. As these parameters are different from NSs, Flores et al. [31] concluded that these new relations can be used to

distinguish BSs from NSs. We note that a is small but negative in the case of BSs, and b is higher compared to the other NS cases.

We reproduce f as a function for $\sqrt{GM/R^3}$ for these cases as reported in Fig.3 of [31] (not shown here). There is a slight uncertainty involved as the curves do not identically overlap. As we discussed in this work, all the quantities scale with x . Hence, we check f' as a function of $\sqrt{M'/R'^3}$. We thus expect a unique relation as these quantities do not depend on the model parameters. This is shown in Fig. 5(a). We perform a linear fit given by

$$f' = -0.0045 + 0.21\sqrt{\frac{M'}{R'^3}} . \quad (4.4)$$

The fit agrees within 2.6%. We refer to the fit coefficients in Eq. 4.4 as $a' = -00045$ and $b' = 0.21$. Writing back in unprimed quantities as given in Eq. 4.3, we get $b = b' = 0.21 = 63.0$ kHz km. Thus, b remains unchanged, and we obtain the same slope. This value is consistent with the one obtained in [31] but is higher compared to the one obtained in [33]. $a = a'/(xM_{Pl}) = 5.67 \times 10^{-7}/(x/\text{MeV}^{-2})$ kHz.

This equation can be used to understand the dependence on these quasi-universal relations as a function of model parameters and explain the little variation obtained in [31]. For NS mass range as considered in [31, 33], $x \approx \Delta x \approx \mathcal{O}(10^{-5})$ MeV $^{-2}$. Differentiating $a = a(x)$ with respect to x , we get $a \approx \Delta a \approx \mathcal{O}(10^{-2})$ kHz, which is approximately the value and error found in the parameter a in [31, 33]. They also report an error in b ; however, from this analysis, we expect b to be invariant. The residual variations could be attributed to numerical error. We can also say that a variation of $\mathcal{O}(0.1)$ or higher in a is expected for $x \lesssim 10^{-6}$. For larger values of x , i.e., BSs with higher maximum masses, the coefficient approaches zero asymptotically.

Another empirical relation for the f -mode damping time exists as a function of compactness when it is scaled by mass and radius [59]. The fit for BSs is given by

$$\frac{R^4}{M^3\tau} = 0.111 - 0.386C . \quad (4.5)$$

where, M , R , C , and τ are mass, radius, compactness and damping time of f -mode oscillations. The coefficients are in close agreement with the recent fit provided by [33]: $\frac{R^4}{M^3\tau} = 0.1105 - 0.3764C$. The relation is invariant under the change to primed quantities. Thus, we directly plot $R^4/M^3\tau$ as a function of C in Fig. 5(b). This is truly a universal relation for massive BSs and is followed no matter what the underlying model parameters are. We show the linear fit given by Eqn. 4.5 with a blue curve. The fit error is within 1.5%. Since the quantities plotted are invariant, we can directly compare them to the corresponding band obtained for NSs [59–61]. This band is shown in grey, and we conclude that BSs have a different relation. This also can be used to distinguish them from NSs. The fit given in [31] is not shown here. Fig. 3 of [31], the compactness goes beyond the value of 0.18. However, the compactness for BSs, in our case, only goes up to 0.16. Also, they use a different fitting relation. Hence, we do make a comparison here.

4.3.2 f -Love- C

There are also other relations involving mass-scaled f -mode characteristics that are universal in nature. The complex eigenfrequency, when scaled with mass, shows a tight correlation with compactness [59, 61]. This fit is of the quadratic form as in Eq. 4.1 with $Y = M\text{Re}(\omega_f)$,

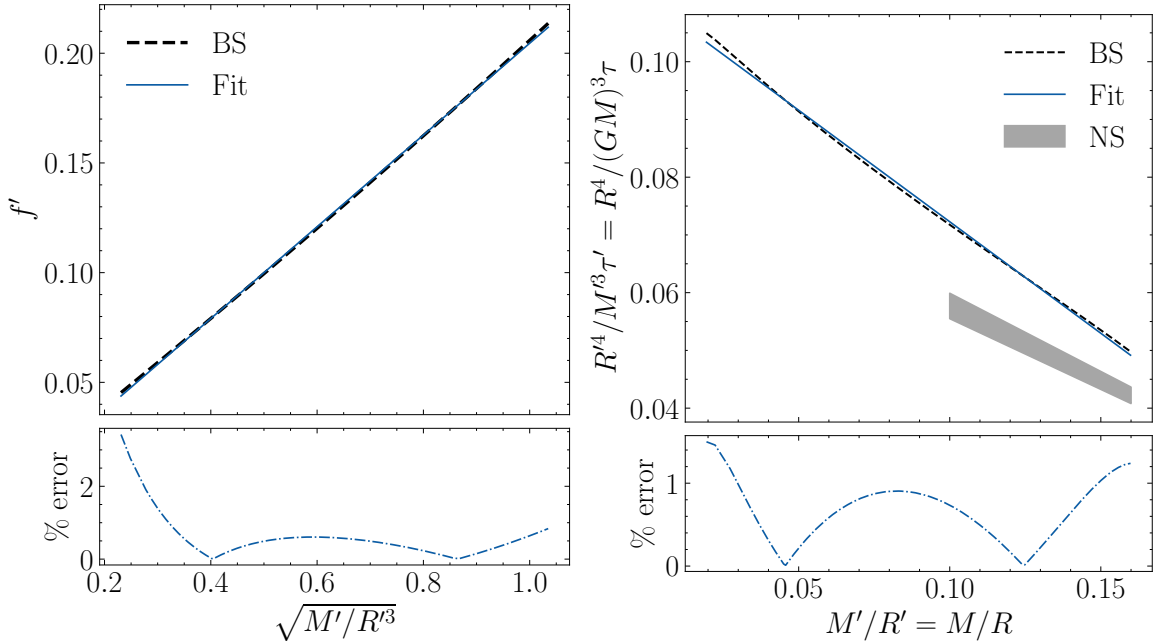


Figure 5. Universal relations connecting (a) f -mode frequency in primed coordinates to the average density of BS and (b) scaled damping time ($R^4/M^3\tau'$) to compactness as suggested in [59]. The grey band is the uncertainty in NSs with and without hyperonic matter. The band spans the fit relations reported in [59–61]. The blue curves are fits given in Eqs. 4.4 and 4.5. The errors in BS fits are shown in lower panels.

$X = C$ and $Y = M\text{Im}(\omega_f)/C^4$, $X = C$. Here, $\text{Re}(\omega_f) = 2\pi f$ is the f -mode angular frequency, and $\text{Im}(\omega_f) = 1/\tau$ is the inverse of damping time. Another universal relation exists between the mass-scaled complex f -mode frequency and the dimensionless tidal deformability [63–65]. The fit is of the quartic form of Eqn. 4.1 with $Y = M\omega_f$ and $X = \ln \Lambda$.

We plot these the relations for $\text{Re}(M\omega_f)$ in Fig. 6 and for $\text{Im}(M\omega_f)$ in Fig. 7 respectively. Note that $M\omega_f = M'\omega'_f$. All these quantities are independent of the model parameters x and, again, are truly universal for the case of massive BSs. These are exact relations with no spread. These can also be compared with the case of NSs. Ref. [61] also obtained such fits using a large set of nuclear and hyperonic EoS. These are plotted in green-dashed lines in all the figures. The relations with the tidal deformability are consistent with the case of NSs. The ones containing compactness, however, show deviation and follow different relations than NSs. The fits for BSs, as obtained in this work, are shown in blue. The fit coefficients are tabulated in Table. 3 We see the f -Love and the $f - C$ fits have an error of less than 0.5% and 1% respectively. For the case of τ relations, the errors are higher, with it being within 4% for $\tau - C$ and as high as 50% for τ -Love.

The quantity $N = f\tau = f'\tau'$ given the number of oscillations that the BS undergoes before its amplitude damp by a factor of e . Again, this quantity does not scale with x . We plot it against C in Fig. 8 (taken from [34]). We see that N decreases with compactness, i.e., more compact configurations for any set of (λ, m) undergo less number of oscillations before damping out. For $C \approx 0.02$, N can be as high as 10,000. For the case of the most compact configuration, we get a minimum number of such oscillations given by $N_{min} = 406$. All BSs oscillate at least N_{min} times within the damping time. This also translates to a high

Y	X	a_0	a_1	a_2	b_0	b_1	b_2	b_3	b_4
$\text{Re}(M\omega_f)$	$\ln\Lambda$	-	-	-	2.365×10^{-1}	-3.753×10^{-2}	2.103×10^{-3}	-4.204×10^{-5}	5.420×10^{-8}
$\text{Re}(M\omega_f)$	C	-0.0024	0.237	1.886	-	-	-	-	-
$\text{Im}(M\omega_f)$	$\ln\Lambda$	-	-	-	2.024×10^{-4}	-5.189×10^{-5}	5.000×10^{-6}	-2.141×10^{-7}	3.428×10^{-9}
$\text{Im}(M\omega_f)/C^4$	C	0.110	-0.362	-0.056	-	-	-	-	-
N	$1/C$	-	-	-	1.833	1.442×10^{-1}	-3.901×10^{-3}	6.121×10^{-5}	-3.879×10^{-7}

Table 3. Fitting coefficients for the f -Love- C universal relations and $N - C$. The fit equations are given in Eqs. 4.1.

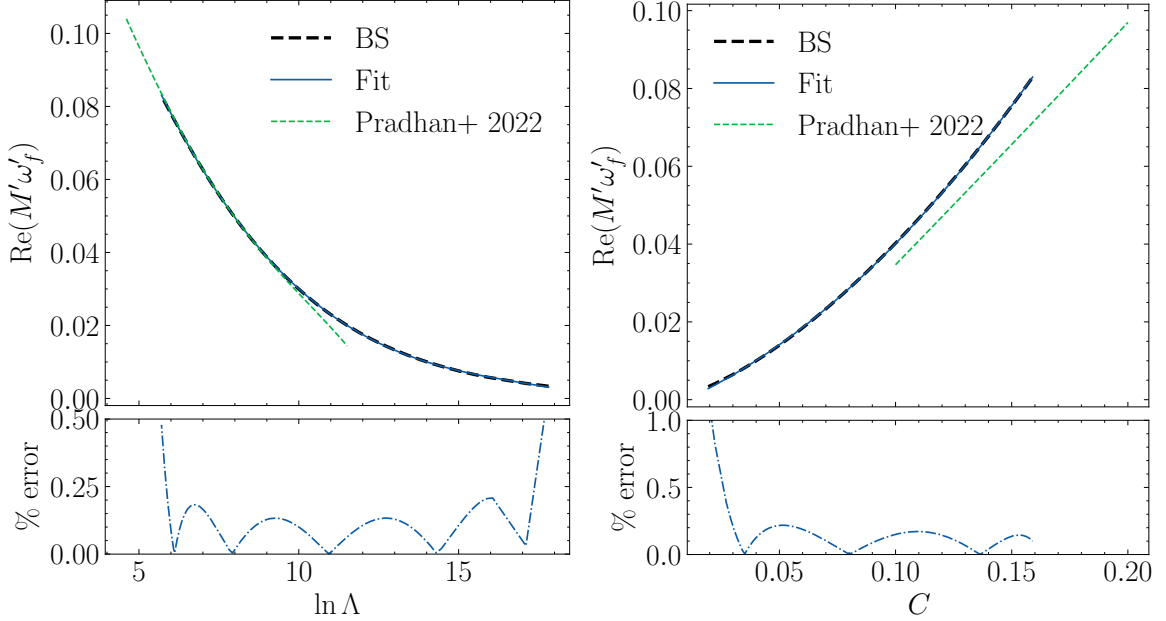


Figure 6. Universal relations for mass-scaled f -mode frequency as a function of the (a) logarithm of the dimensionless tidal deformability and (b) compactness. The fits are shown in blue, whose fitting coefficients are provided in Table. 3. The corresponding percentage errors are shown in the bottom panels. The relations followed by NS and hyperonic NSs are shown in green [61]

quality-factor ($Q = \pi f \tau$) of GW waveform, which will be discussed later in Sec. 4.5. We show a quartic polynomial (Eqn. 4.1) fit in blue. The fit has a percent error below 2%. The fit coefficients are reported in Table. 3.

4.4 Observable parameter space

In this section, we focus on the scalar DM parameter space. We discussed various constraints in Sec. 3, and the available parameter space is visually shown in Fig. 1. For this entire region, it would be interesting to obtain the information of f -mode characteristics.

First, we show the same parameter space with the constraints in Fig. 9. For every set of parameters (m, λ), we can compute the maximum possible f -mode frequency (f_{max}), corresponding to the most compact configuration. We can see that f_{max} is higher for larger DM mass (m) and for smaller values of self-interaction (λ). Thus, the trend is inverse to that of the maximum mass M_{max} . This trend is clear from the scaling relation $f_{max} = 0.21/(xM_{Pl}) = (0.21/M_{Pl})(m^2/\sqrt{\lambda})$. The variation is over orders of magnitude; hence we show all the quantities in log scale.

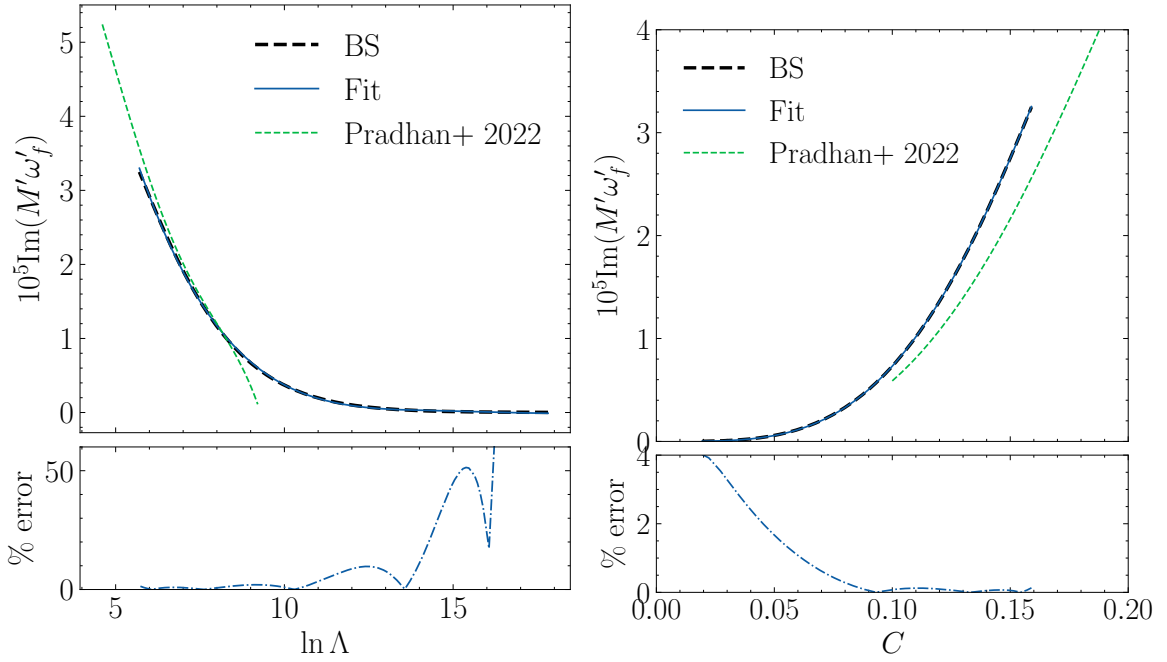


Figure 7. Same as Fig. 6 but for the f -mode damping time

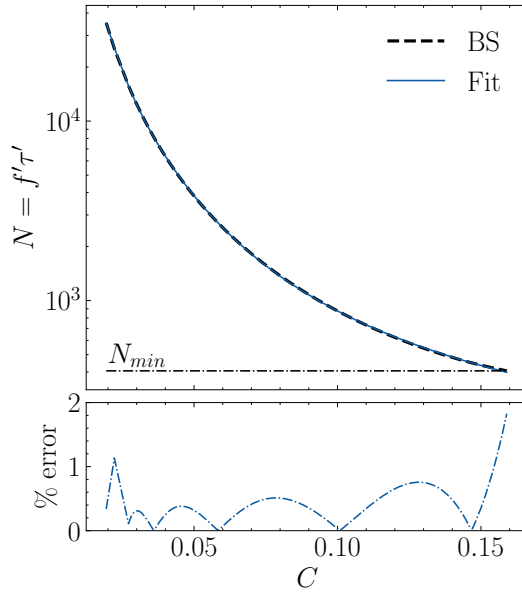


Figure 8. Number of cycles ($N = f\tau = N'\tau'$) completed by BSs within damping time. BSs complete a minimum of $N_{min} = 406$ oscillations for the case of the highest compactness configuration. The analytical fit is shown in blue, whose fitting coefficients are provided in Table. 3. The corresponding percentage error is shown in the bottom panels

From an observation point of view, it would be of great interest to know what region of this vast parameter space could actually be accessible in the near future. f -mode oscillations of BSs would result in the emission of GW of f -mode frequencies. Hence, for reference, we

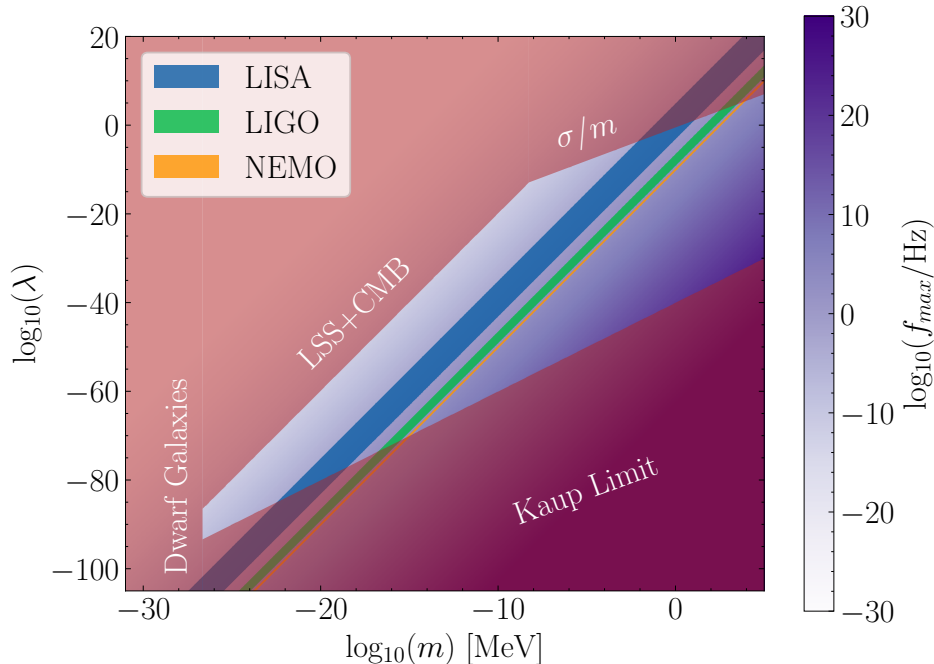


Figure 9. The maximum f -mode frequency for the entire parameter space for BSs. The colour indicates the $\log_{10}(f_{max})$ in Hz. The constraints from Fig. 1 are used to mask the excluded region in red. Only the unmasked region is relevant to the analysis. The frequency sensitivity bands for LIGO (green) and two of the future detectors, LISA (blue) and NEMO (orange) are shown. The frequency sensitivity assumed for LISA is 0.1 mHz - 1Hz, [50-1000] Hz for LIGO, and [2-4] kHz for NEMO. The region to the right of each band is sensitive to each detector.

plot the frequency band sensitive to various current and future GW detectors. We show the bands for three detectors, LISA, LIGO, and NEMO, in Fig. 9 in blue, green, and orange, respectively. The frequency sensitivity assumed is [0.1 mHz, 1 Hz] for LISA, [50, 1000] Hz for LIGO, and [2, 4] kHz for NEMO. These bands can be used as iso-contours for f_{max} in the plot. The bands for Cosmic Explorer (CE) and Einstein Telescope (ET) are not explicitly shown. Their sensitivity bands encompass those of the LIGO and NEMO and further push down in the lower frequency range of a few Hz. Thus, all the GW detectors together roughly cover the region bounded by the blue and orange bands.

It is important to note that since we are plotting the maximum f -mode frequency here, it does not mean that these are the only bands that can be probed. The region towards the right of these bands has f_{max} larger than the sensitivity range, i.e., the frequency of a configuration with lower compactness for these parameters can still fall in the detection band. Hence, in principle, the entire parameter space falling to the right of the band for each detector can be probed by that detector. This idea will be made clearer later when we show the exact masses and compactness that these GW detectors can probe.

Since we know that the f_{max} scales with a particular combination of (m, λ) , which is given by $f_{max} \propto m^2/\sqrt{\lambda} = 1/x$, it is more meaningful to focus on the parameter x and obtain the range of x that can be probed. In Fig. 10, we show this relation of f_{max} on x in a black line. All axes are in log scale. f_{max} decreases with x . The bands for the three detectors, as discussed, are shown in the same colour. Note that the black line marks the upper limit on frequency. We show x here in the range $[10^{-6}, 10^3]$ MeV^{-2} . For lower values of x , the

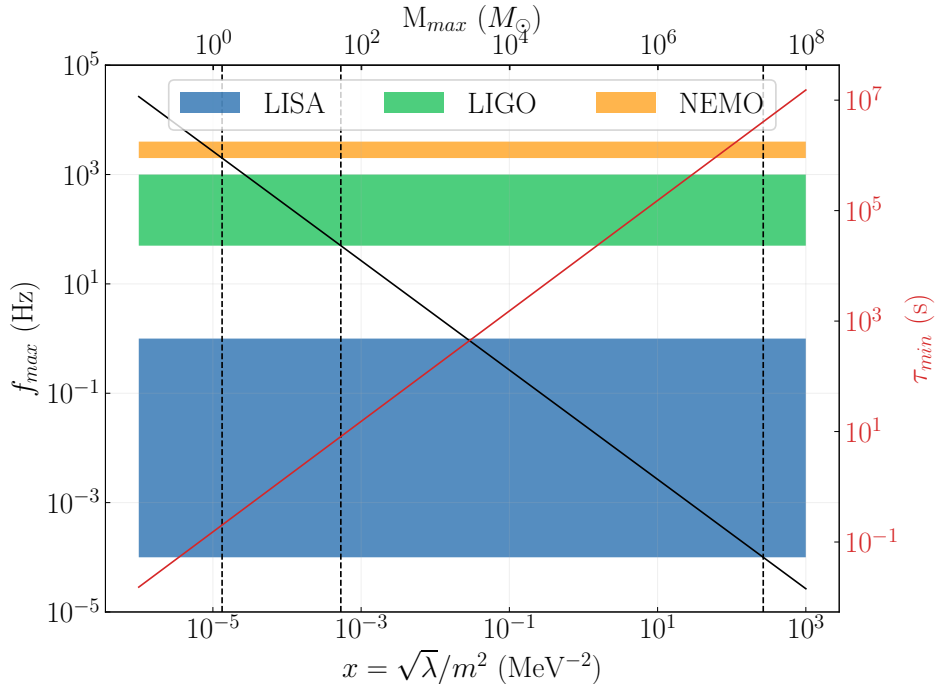


Figure 10. Maximum f -mode frequency (black) and minimum damping time (red) as a function of scaling parameter. The corresponding maximum mass possible is shown on the upper axis. The frequency bands for LIGO and future planned GW detectors LISA and NEMO are shown in great, blue, and orange bands, respectively. The frequency sensitivity assumed for LISA is 0.1 mHz - 1Hz for LISA, [50, 1000] Hz for LIGO, and [2, 4] kHz for NEMO. The vertical dashed lines indicate the upper limit on x that can be probed by NEMO, LIGO, and LISA, as we go from left to right. For higher values of x , the maximum f -mode frequency falls below the detector sensitivity range. The three values are $1.33 \times 10^{-5} \text{ MeV}^{-2}$, $5.32 \times 10^{-4} \text{ MeV}^{-2}$, and $2.66 \times 10^2 \text{ MeV}^{-2}$ for NEMO, LIGO, and LISA, respectively.

compactness of BS would have to be too low to be detectable. We will show this in the next plot. We see that at $x = 10^3 \text{ MeV}^{-2}$, the black line is already below the frequency range of all detectors and is not observable. The point where the black line goes below this detection threshold is $x_{thresh} = 2.66 \times 10^2 \text{ MeV}^2$. This is shown by the rightmost black-dashed line in the figure. This is an absolute upper threshold on x , such that $x > x_{thresh}$ is not accessible to the currently planned GW detectors. This threshold is set by the one observing in the lowest frequency range, i.e., LISA. The Pulsar Timing Array (PTA) observes GW in nano-Hz frequencies but is restricted to stochastic GW. Hence, we have not considered it here.

Similar upper thresholds can be obtained for other detectors as well. For LIGO, the threshold is $x \leq 5.32 \times 10^{-4} \text{ MeV}^{-2}$ while for NEMO it is $x \leq 1.33 \times 10^{-5} \text{ MeV}^{-2}$. If we consider the proposed deci-HZ detectors [66, 67] that are expected to be sensitive in [0.1, 10] Hz range, we obtain $x \leq 0.266 \text{ MeV}^{-2}$. In principle, the region $x \leq 1.33 \times 10^{-5} \text{ MeV}^{-2}$ is accessible to all detectors.

On the same plot, we show some more information. As seen before, we can also calculate the minimum value of the damping time for a given x as $\tau_{min} = 1900xM_{Pl}$. We show this by the red curve, and the axis is marked on the right side of the figure. Since damping time is not easily measurable, we focus on the frequency for the rest of the study. On the

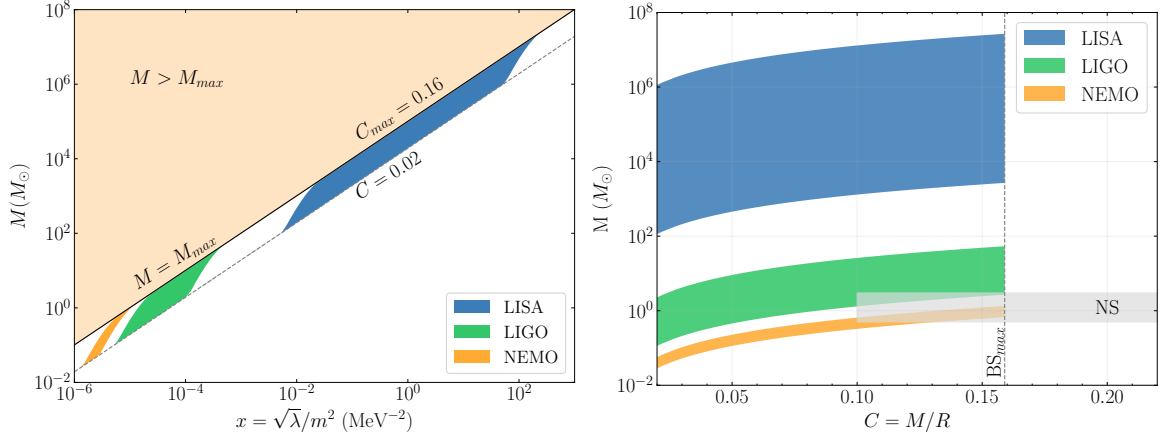


Figure 11. (a) Masses of BSs falling in various GW bands for a given set of model parameters x . (b) Mass and compactness of BSs that could be probed by LIGO and planned future detectors LISA and NEMO. The mass-compactness range for NSs is marked by the grey patch. The frequency sensitivity assumed for LISA is 0.1 mHz-1Hz for LISA, [50, 1000] Hz for LIGO, and [2, 4] kHz for NEMO. The NS mass-compactness range is marked by the silver patch.

upper axis, we show the values of maximum mass corresponding to the values of x given by $M_{max} = 0.06xM_{Pl}^3$. This figure compares the maximum frequency with the GW detector bands and marks the maximum mass of BS that would be observable. The threshold on x would change if we considered BSs of lower compactness. In general, we would like to see the actual ranges of mass and x that can be probed. This is studied in detail in the following subsection.

In Fig. 11(a), we show the mass range corresponding to various values of x that can be probed by the same GW detectors. The black line marks the maximum possible mass for a given value of x ($M = 0.06xM_{Pl}^3$), which also corresponds to the maximum compactness case. The region above this is inaccessible as we enter the unstable branch. These masses are expected to collapse to a BH. The dashed line marks the mass of BSs having $C = 0.02$. As $M'(C = 0.02) \approx 0.012$, this corresponds to $M = 0.012xM_{Pl}^3$. As we solve for f -modes only for $C \gtrsim 0.02$, we only focus on the regions between these two lines. Using the $f' - M'$ relation (Eq. 4.2), we can use the scaling to write $f = f(x, M)$. Doing this, for each (x, M) in this region, we can check if the f -mode frequency falls in any of the GW detectors bands. The region in (x, M) falling in LISA, LIGO, and NEMO bands are shown in blue, green, and orange, respectively. Thus for each x , we get a range in mass that can be probed. We see that BSs roughly in the mass range of $10^2 - 10^7 M_\odot$ are observable by LISA, $0.1 - 10 M_\odot$ by LIGO and $0.01 - 1 M_\odot$ by NEMO. Note that for each case, we can probe even lower masses if we consider BSs with compactness lower than 0.02.

To get a more physical picture, in Fig. 11(b), we show the same information in the $M - C$ plane. We make use of Eq.14 of [34] for obtain $f = f(C, M)$. Thus for each (C, M) we can compare the BS f -mode frequency with various detector bands. The compactness varies between 0.02 and 0.16, the maximum for BS. We conclude that a mass range lower than that corresponding to C_{max} can be probed for low compactness configurations. In this place, we can make a direct comparison with NSs as they typically lie within 1-3 M_\odot and have compactness in the range 0.1-0.3. BHs fall on the extreme right of this diagram at $C = 0.5$.

4.5 Detectability

We consider a model for burst GW as considered in [68], where oscillations are excited in a BS at $t = 0$. We do not know any of any mechanisms that can excite f -mode oscillations for an isolated BS. The possible mechanisms to excite these could be i) during the formation of BS (like gravitational cooling) or ii) nearby astrophysical objects that hit the BS or interact closely (external perturbations). Here, we assume the oscillations are excited without delving deep into the excitation mechanism. We analyze the detectability assuming f -modes are excited. The oscillation frequency is its fundamental frequency f , which damps with a timescale of τ as it radiates GW. The GW strain amplitude $h(t)$ for such a signal is given by

$$h(t) = \begin{cases} 0 & t < 0 \\ h_0 e^{-t/\tau} \sin(2\pi ft) & t \geq 0 \end{cases} \quad (4.6)$$

Here, h_0 is the peak amplitude measured by the GW detectors. It can be related to the total energy in the oscillations that is radiated away E , the distance of the detectors from the source of burst d , and the f -mode characteristics f and τ . This is given by [68, 69]

$$h_0 = \frac{1}{\pi df} \left(\frac{5G E}{c^3 \tau} \right)^{1/2} = 1.53 \times 10^{-17} \left(\frac{1 \text{ kpc}}{d} \right) \left(\frac{E}{M_\odot} \right)^{1/2} \left(\frac{1 \text{ kHz}}{f} \right) \left(\frac{1 \text{ s}}{\tau} \right)^{1/2}. \quad (4.7)$$

The signal-to-noise ratio or SNR (ρ) for such a burst signal is derived as [70, 71]

$$\rho = \sqrt{\frac{4Q^2}{1 + 4Q^2}} h_0 \sqrt{\frac{\tau}{2S_n}}. \quad (4.8)$$

Here, Q is the quality factor of the signal given by $Q = \pi f \tau$. This roughly gives the number of cycles (N) of the burst oscillations before the amplitude falls by a factor of e . We saw in Fig. 8 that N_{min} for BSs is 406. This means that $Q \geq 406\pi$, which means $4Q^2 \gg 1$. Thus, the SNR for BSs simply reduces to

$$\rho = h_0 \sqrt{\frac{\tau}{2S_n}}. \quad (4.9)$$

S_n is the noise spectral density of the detector at the frequency of evaluation f .

We use Eq. 4.9 to calculate the SNR.

$$\rho = 1.08 \times 10^{-17} \left(\frac{1 \text{ kpc}}{d} \right) \left(\frac{E}{M_\odot} \right)^{1/2} \left(\frac{1 \text{ kHz}}{f} \right) \left(\frac{\text{Hz}^{-1/2}}{\sqrt{S_n}} \right) \quad (4.10)$$

$$= 1.08 \times 10^{-17} \left(\frac{1 \text{ kpc}}{d} \right) \left(\frac{E}{M_\odot} \right)^{1/2} \frac{1}{202.67 f'(C) M'(C)} \left(\frac{M_{BS}}{M_\odot} \right) \left(\frac{\text{Hz}^{-1/2}}{\sqrt{S_n}} \right) \quad (4.11)$$

$$\rho = 4.23 \times 10^{-23} E_d \left(\frac{M_{BS}}{M_\odot} \right)^{3/2} \left(\frac{0.21}{f'(C)} \right) \left(\frac{0.06}{M'(C)} \right) \left(\frac{\text{Hz}^{-1/2}}{\sqrt{S_n}} \right). \quad (4.12)$$

We have used the relation reported in [34] to write f in terms of M and C . This relation of BS SNR is completely in terms of E , d , M , and C and does not include any explicit dependence on the f -mode characteristics. We have defined the parameter E_d as

$$E_d \equiv \frac{\sqrt{E/(10^{-10} M_{BS})}}{d/(1 \text{ kpc})}. \quad (4.13)$$

We have used a factor of $10^{-10}M_{BS}$ as a normalization of the energy emitted by the f -modes. Thus, $E_d = 1$ means an energy corresponding to 10^{-10} times that of the mass-energy of the BS is radiated at a distance of 1 kpc. Or alternatively, an energy of $n \times 10^{-10}M_{BS}$ radiated at a distance of \sqrt{n} kpc. We also note that the SNR for a fixed E_d grows with M_{BS} . The primary reason for this is that the f -mode frequency for fixed compactness goes as the inverse of mass, and lower frequency results in larger signal strength.

In a realistic scenario, BSs in the universe might have different compactness depending on the initial formation conditions, but the model parameters are expected to be fixed. Thus, DM would have a fixed value of x , and compactness could be anything depending on the mass of the BS that formed. Hence, it is more natural to think in terms of C - x parameters. Hence, we also provide the expression for $\rho(x, C)$ here. We can write $M_{BS} = M'(C)xM_{Pl}^3$. Doing this we get

$$\rho = 1.30 \times 10^{-15} E_d \left(\frac{x}{\text{MeV}^{-2}} \right)^{3/2} \left(\frac{0.21}{f'(C)} \right) \left(\frac{M'(C)}{0.06} \right)^{1/2} \left(\frac{\text{Hz}^{-1/2}}{\sqrt{S_n}} \right). \quad (4.14)$$

Now, we set $\rho \geq 5$ as a threshold for detection. This gives us

$$E_d \geq 3.85 \times 10^{15} \left(\frac{\text{MeV}^{-2}}{x} \right)^{3/2} \left(\frac{f'(C)}{0.21} \right) \left(\frac{0.06}{M'(C)} \right)^{1/2} \left(\frac{\sqrt{S_n(f(x, C))}}{\text{Hz}^{-1/2}} \right). \quad (4.15)$$

The equality gives the minimum values of E_d ($(E_d)_{min}$) required for the BS burst source of compactness C made of DM with parameter x that is detectable with an SNR of 5 by a GW detector with the noise spectral density S_n . The lower the value of $(E_d)_{min}$, the better the detectability. We expect this to be better for LISA as the SNR is higher for lower frequency (or higher mass).

In Fig. 12(a) we plot this $(E_d)_{min}$ (shown in colour) as a function of x and C for the case of advanced LIGO (aLIGO). x and $(E_d)_{min}$ are shown on log scales. The SNR and $(E_d)_{min}$ depends on f . f in turn depends on both x and C . Since we are plotting x on a log scale, the frequency, too, varies on a log scale here along the x-axis and increases along decreasing x and increasing C . The parameter space shown for aLIGO covers frequencies in the range of 5-5000 Hz. We observe that detectability is better for lower frequencies (high x and low C). The dark strip seen at the bottom right is due to the higher noise for aLIGO around 9.7 Hz. This worsens the detectability. We observe very high values for $(E_d)_{min}$. $\log_{10}(E_d)_{min} \gtrsim 9$ in the best case scenario.

As the SNR is better for lower frequencies and higher BS mass, the detectability is expected to be the best in the case of LISA, as it is planned to be observed in the millihertz range. We make the same plot for the LISA detector (see Fig. 12(b)). The range of x is such the frequencies fall in the LISA band, i.e., 0.1 mHz - 1Hz. We see that in this range $\log_{10}(E_d)_{min} \gtrsim 4$. This means that for $E = 10^{-10}M_{\odot}$, the distance of BS has to be $x \lesssim 0.1$ pc, i.e., roughly the size of Oort cloud. In the theoretical limiting case of $E = M_{BS}$, we reach the approximate distance of the galactic center from the Sun ≈ 10 kpc. However, this is an unrealistic case. Thus, in the best possible case, we would be able to detect f -modes from BSs in the Solar System neighbourhood.

The same range as that of aLIGO is probed by the CE and ET detectors. We expect better sensitivity with next-generation detectors as they have an order of magnitude improved sensitivity. We show the same plots of CE and ET in Fig. 13. A fainter band in the dark region on the CE plot is due to a dip in the noise at around 4kHz, improving the detectability.

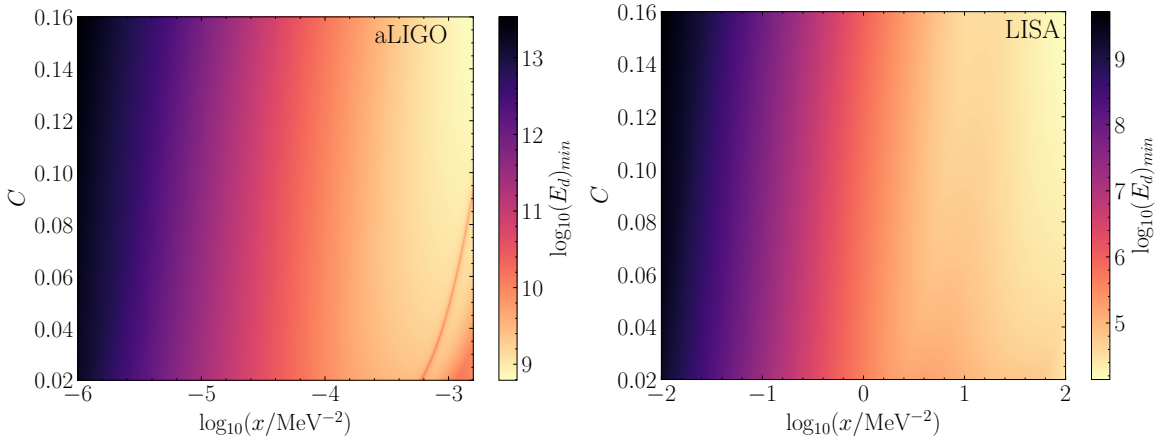


Figure 12. The detectability of BSs using (a) aLIGO and (b) LISA GW detectors. The colours indicate the minimum values of E_d required for the detection with $\rho \geq 5$. The sensitivity curve for aLIGO is obtained from <https://dcc.ligo.org/LIGO-T1500293/public>. For LISA, the sensitivity curve was constructed using the analytical fit provided in [72]. The range for x probed is different as aLIGO noise spectral density used is in the range 5-5000 Hz and 0.1 mHz - 1 Hz for LISA.

We also see a few very fine dark lines in the case of ET, all being due to narrow spikes in the noise spectral density. We see that detectabilities of CE and ET are comparable with $\log_{10}(E_d)_{min} \gtrsim 7.8$. This improvement in order of magnitude compared to aLIGO is expected as $(E_d)_{min} \propto \sqrt{S_n}$, and $\sqrt{S_n}$ is lower by an order of magnitude. Thus, in the LIGO frequency range corresponding to stellar mass BS, we have $\log_{10}(E_d)_{min} \gtrsim 7.8$. Overall, these are very large values for $(E_d)_{min}$ from a detectability point of view. $(E_d)_{min} = 8$ means for $E = 10^{-10} M_\odot$, the distance to the BS has to be less than 10^{-8} kpc or ≈ 2 AU. This means detectability only extends to near-Earth BS or to BSs within the solar system for higher burst energies. For these detectors, we have seen that relevant BS masses are 0.1-10 M_\odot . In the theoretical limiting case of $E = M_{BS}$, which is unrealistic, we reach the distance of the nearest star ≈ 1 pc.

5 Discussions

5.1 Summary

In this work, we have focussed on a class of dark stars called dark stars made of scalar bosons. This is modelled by a scalar field ϕ that interacts gravitationally with all matter and with itself depending on the potential $V(\phi)$. We focus on the simplest potential given by $V(\phi) = \frac{1}{2}m^2\phi^2 + \frac{1}{4}\lambda\phi^4$. The strong-interaction limit ($\Lambda = \lambda M_{Pl}^2/4\pi m^2 \gg 1$) results in the formation of a “massive star” whose mass scales as $\propto \sqrt{\lambda} M_{Pl}^3/m^2$ resembling massive fermionic stars. We study the non-radial f -mode oscillations of such massive BSs and the implications of scaling relations reported in [34].

Scalar DM parameter space: We display the entire parameter space available for massive BSs and review all the available and relevant constraints. The astrophysical observations provide upper limits on λ as a function of mass. A recent model independent study [40] gave a lower limit of scalar DM mass. Moreover, We stay in the $\Lambda \gg 1$ (put lower bound on λ for the scalar DM to form massive BSs.

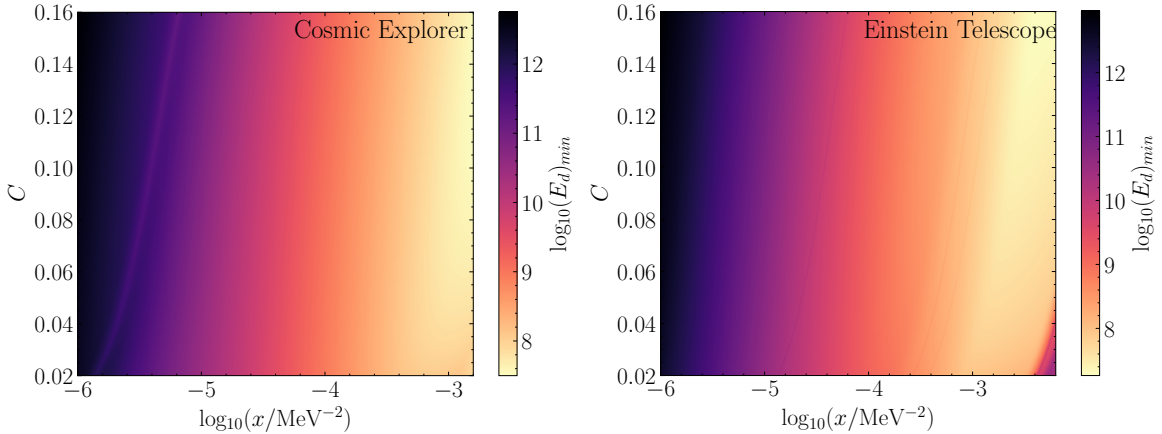


Figure 13. The detectability of BSs using (a) Cosmic Explorer and (b) Einstein Telescope GW detectors. The colours indicate the minimum values of E_d required for the detection with $\rho \geq 5$. The sensitivity curve for CE is obtained from <https://dcc.cosmicexplorer.org/CE-T2000017/public> and from <https://dcc.ligo.org/LIGO-T1500293/public> for ET. The range for x probed is different as CE noise spectral density used is in the range 5-5000 Hz and 1 Hz - 10 kHz for ET.

Static properties: Mass and radius of massive BSs scale with the parameter $x = \sqrt{\lambda}/m^2$. Thus, relations between scaled mass M' , scaled radius R' , and $C' = C$ are independent of the model parameters. We provide analytical fit functions (quadratic and quartic polynomials) along with fit coefficients and errors for the $M' - C'$, $R' - C'$, and $M' - R'$ curves and report the corresponding errors. The quartic fits are more accurate as expected, with an accuracy of $\lesssim 0.75\%$. The fits are very useful for future works of massive BS as direct analytical expressions can be used to calculate static observables instead of numerical solutions. We also find that the maximum density that can be reached at the centre of a stable BS is $\rho'_c = 1.6$.

f-modes: We then evaluate the f -mode characteristics for massive BSs using a full general-relativistic setup. We use the f -mode frequency and damping time scaling relations as reported in [34]. We report analytical fits for the $f' - M'$, $f' - C'$, and $\tau' - M'$, $\tau' - C'$ relations, which can be used to evaluate the f -mode characteristics for any parameter values in the available parameter space along with the corresponding errors. All the fits are accurate to within 5% and can be directly used in future works concerning f -modes of massive BSs without the need for any numerical calculations.

Empirical relations: We then study the known empirical and quasi-universal relations for f -modes that are essential to probe the properties of interior matter. We showed that since scaling takes away the EoS dependency, we get a unique relation for $f' = f'(\sqrt{M'/R'^3})$ and $R'^4\tau'/M'^3 = \tau'(M'/R')$. We provide linear fits to both that agree within 3%. The τ' relation is found to be universal for BSs; however, it deviates from that for NSs.

Universal relations: We also check the well-known universal relation of the mass-scaled f -mode characteristics with the dimensionless tidal deformability and compactness. These relations are well-studied for NSs [58–60, 73, 74], as well as NSs containing hyperons [61, 75, 76], deconfined quark matter [77–81], and DM-admixed NSs [82–86]. All these quantities, $M'f'$, M'/τ' , Λ , C do not scale with x . Hence, we get unique $M'\omega_f - \Lambda$ and $M'\omega_f - C$ for both the real and imaginary parts of the complex eigenfrequency, making it an exact relation for BSs. We report these relations here, along with corresponding analytical fits and errors.

We also compare it with NS fits and find that the fits involving compactness deviate for BSs. We also report the fit for $N = f\tau = f'\tau'$ as a function of compactness, representing the number of cycles before the QNM damps e -folds.

Observable parameter space: Focussing on the observational aspects of these f -modes for BSs shows the maximum possible f -mode frequency for each set of parameters (λ, m) of DM, spanning the entire available parameter space. Using the frequency range of current and future GW detectors, we show what DM parameters space can be probed by the LISA, LIGO, and NEMO detectors. The space probed by ET and CE would span the region probed by LIGO and NEMO. We derived an upper limit of x given by $x_{thresh} = 2.66 \times 10^2 \text{ MeV}^2$ such that model parameters with $x > x_{thresh}$ cannot be probed by any GW detector.

Detectability: To check the detectability, we explore the $C - x$ parameters space, which represents a BS of compactness C given the DM model parameters. For each point in this space, we calculate the lower bound on a quantity $E_d \equiv \sqrt{E}/d$ demanding that the SNR for the f -mode burst is $\gtrsim 5$. We find that for the f -mode energy of $E \approx 10^{-10} M_{BS}$, BSs within the solar system would be accessible to next-generation GW detectors like CE and ET. The detectability of BS f -modes is much better in the case of LISA, and BSs can be probed in the solar neighbourhood.

5.2 Comparison with other works

Static observables: Colpi et al. [12] first showed that in the strong-interaction limit, the EoS and, hence, the mass-radius curves are independent of the DM model parameters. Following this, many works have used this fact, but simple analytical expressions connecting mass, radius, and compactness were not available. Tang et al. [53] provided multiple fits for different mass regions for mini BS, i.e., in the Kaup limit. A relation between mass-compactness was reported in Pacilio et al. [56]. Using this and the $\Lambda - M$ relation reported in Sennett et al. [57], they also derived the $k_2 - M$ relation. We update all these relations in this work.

Maselli et al. [41] showed that massive BSs follow the I -Love- Q relations for select values of model parameters in the NS mass range. Wu et al. [87] also showed this for a few BS models. In this work, we explicitly prove that such universal relations are expected as the quantities do not scale with model parameters. We show this for I -Love- C relations and do not consider the spin-induced quadrupole moment here as we restrict the non-spinning case, also providing a comparison with NSs.

Sennett et al. [57] reported that Λ_{min} for BSs is 280. A recent work by Cipriani et al. [21] reported $\Lambda_{min} \approx 290$ and $k_{2,min} \approx 0.045$. Our results are consistent as we obtain $\Lambda_{min} = 280$ and $k_{2,min} = 0.045$. Cardoso et al. [88] studied tidal deformability in detail. The minimum value for the BSs considered here was not explicitly reported.

BS QNMs: [27] studied BS QNMs for odd parity, which have been shown not to couple to gravitational radiation. [28] explored the even parity QNM in detail, however, the work is restricted to non-interacting case ($\Lambda = 0$). [29] explore QNMs of self-interacting BSs restricting themselves to weak-interaction limit ($\Lambda < 200$) and do not focus on the damping times. [30] carry out a similar analysis but for three types of cases (Mini BS, Massive BS, and Solitonic BS). For the case of massive BS, as discussed in this work, they fix $\Lambda = 200$, again in the weak interaction limit. The dimensionless quantity used was $\omega' = \omega/m$ as opposed to $\omega' = \omega\sqrt{\lambda}/m$ in our case. Thus, we cannot compare our results with those of these works. [32] studied radial QNMs, which do not give out GWs.

Massive BS QNMs in the strong-interaction limit: Flores et al. [31] first explored non-radial fundamental modes for massive BSs in the strong-coupling limit in detail. They con-

sidered select parameter values consistent with the σ/m constraints on self-interacting DM and only restricted the work to BSs falling in the mass range of $1-6M_{\odot}$ and found that the f -mode characteristics of BSs in this mass range follow the empirical universal relations that are different from those followed by NSs. These are consistent with our findings. We showed in [34] that scaling relations can be used to compute f -mode characteristics for any model parameters using a single solution. There is no need to study f -modes separately for different parameter values. Using this, we also show why the empirical fits are expected to follow in this case and compare it with the case of NSs. We also include the f -Love-C universal relations in our work and extend the work to comment on the range of parameter space that current and future GW detectors can probe and explore detectability. Another work [33] appeared recently as this work was being carried out. It explored the f -mode universal relations for select model parameters. They also explored the f -mode universal relations involving the moment of inertia.

Observations: On the observational front, [89, 90] provided an in-depth review of various observational signatures of ECOs using GW focussing on the inspiral phase of binary systems and detectability using LIGO was discussed. These were extended to include additional interaction terms [91] and for extreme mass ratio inspiral [92]. [34] extended this list to include quasinormal oscillations. Here, we discuss the detectability as well as parameter space and mass-compactness regions that can be probed using f -modes, in particular, that could also be excited in isolated BS using LIGO as well as future next-generation GW detectors.

5.3 Future Scope

Having derived the scaling and fit relations for non-radial f -mode oscillations, these can be used for the searches of massive BS on the strong-interaction limit where the effect of f -modes is important. These would be relevant in the future when f -mode oscillations become detectable. f -modes for BSs with different interaction potentials, like ϕ^n [93] or axion potentials, vector bosons, as well as other types of ECOs [5] need to be explored further in a similar way.

Stochastic GW background from binary systems of ECos [94], BSs [95], and other exotic sources [96] are also interesting prospects. The recent detection of stochastic GW by the IPTA has restored interest in stochastic GW sources. We found that we could have long-lived low-frequency f -modes for massive BSs depending on the DM model parameters. These BS oscillations could act as an additional source of the stochastic background. .

A Scaling of Love equations

It is known that the Tolman-Oppenheimer-Volkoff (TOV) equations when written in terms of scaled parameters along the EoS, are independent of m and λ (see Appendix of [41]). The same holds for tidal deformability. This was shown in [57] that in the strong-interaction limit, the $\Lambda - M'$ curves remain unchanged. We explicitly show and prove here that the solutions of electric and magnetic tidal love numbers are independent of model parameters when scaled dimensionless quantities are used.

The tidal field consists of two parts [97] i) electric (even parity/polar) (ϵ_L) and ii) magnetic (odd parity/axial) (M_L). The corresponding mass multipole (Q_L) and current multipole (S_L), which is purely GR effect, are related by the equations

$$Q_L = \lambda_l \epsilon_L , \quad (\text{A.1})$$

$$S_L = \sigma_l M_L , \quad (\text{A.2})$$

where, L are the space indices and l is the order of multipole moment. Here, λ_l and σ_l are called the gravitoelectric and gravitomagnetic tidal deformability. Dimensionless tidal deformabilities (Λ_l, Σ_l) are defined by dividing them by a factor GM^{2l+1} . These are given by

$$\Lambda_l = \frac{2}{(2l-1)!!} k_l \left(\frac{R}{GM} \right)^{2l+1} = \frac{2}{(2l-1)!!} \frac{k_l}{C^{2l+1}} , \quad (\text{A.3})$$

$$\Sigma_l = \frac{1}{4(2l-1)!!} j_l \left(\frac{R}{GM} \right)^{2l+1} = \frac{1}{4(2l-1)!!} \frac{j_l}{C^{2l+1}} \quad (\text{A.4})$$

$$(\text{A.5})$$

where k_l and j_l are the gravitoelectric and gravitomagnetic tidal Love numbers. These dimensionless tidal deformabilities depend on the EoS and on the mass configuration via the Love numbers and C . We want to see the effect of EoS on this, so we write the equations in terms of scaled quantities. We have already seen that when written in terms of scaled quantities $C = C'$. The dimensionless tidal Love numbers are purely a function of dimensionless compactness and a dimensionless quantity y given by [97]

$$k_l = k_l(C, y_l) , \quad (\text{A.6})$$

$$j_l = j_l(C, \tilde{y}_l) . \quad (\text{A.7})$$

which are given by

$$y_l = \frac{R}{H_l(R)} \frac{dH_l(R)}{dR} , \quad (\text{A.8})$$

$$\tilde{y}_l = \frac{R}{\tilde{H}_l(R)} \frac{d\tilde{H}_l(R)}{dR} \quad (\text{A.9})$$

Here, R is the radius of the star. The functions H_l and \tilde{H}_l are obtained by solving the

equations [97]

$$\begin{aligned} \frac{d^2 H_l(r)}{dr^2} + \frac{dH_l(r)}{dr} \left(1 - 2\frac{Gm(r)}{r}\right)^{-1} \left[\frac{2}{r} - \frac{2Gm(r)}{r^2} - 4\pi Gr(\rho(r) - p(r))\right] \\ + H_l(r) \left(1 - 2\frac{Gm(r)}{r}\right)^{-1} \left(4\pi G \left[5\rho(r) + 9p(r) + \frac{dp}{dp}(\rho(r) + p(r))\right] \right. \\ \left. - \frac{l(l+1)}{r^2} - 4 \left(1 - \frac{2Gm(r)}{r}\right)^{-1} \left(\frac{Gm(r)}{r^2} + 4\pi Grp(r)\right)^2\right) = 0, \end{aligned} \quad (\text{A.10})$$

$$\begin{aligned} \frac{d^2 \tilde{H}_l(r)}{dr^2} - \frac{d\tilde{H}_l(r)}{dr} \left(1 - 2\frac{Gm(r)}{r}\right)^{-1} 4\pi Gr(\rho(r) + p(r)) \\ - \tilde{H}_l(r) \left(1 - 2\frac{Gm(r)}{r}\right)^{-1} \left(\frac{l(l+1)}{r^2} - \frac{4Gm(r)}{r^3} + 8\pi G\theta(p(r) + \rho(r))\right) = 0. \end{aligned} \quad (\text{A.11})$$

Here, $c = 1$ and $G = 1/M_{pl}^2$. Here $\theta = +(-)1$ for purely static (irrotational) fluid. We now transform to scaled variable $r = r'xM_{pl}$, $m = m'xM_{pl}^3$, $\rho = \rho'/x^2$, and $p = p'/x^2$ as discussed in Sec. 2. Then, these equations become

$$\begin{aligned} \frac{d^2 H_l(r')}{dr'^2 x^2 M_{pl}^2} + \frac{dH_l(r')}{dr' x^2 M_{pl}^2} \left(1 - 2\frac{m'(r')}{r'}\right)^{-1} \left[\frac{2}{r'} - \frac{2m'(r')}{r'^2} - 4\pi r'(\rho'(r') - p'(r'))\right] \\ + \frac{H_l(r')}{x^2 M_{pl}^2} \left(1 - 2\frac{m'(r')}{r'}\right)^{-1} \left(4\pi \left[5\rho'(r') + 9p'(r') + \frac{dp'}{dp'}(\rho'(r') + p'(r'))\right] \right. \\ \left. - \frac{l(l+1)}{r'^2} - 4 \left(1 - \frac{2m'(r')}{r'}\right)^{-1} \left(\frac{m'(r')}{r'^2} + 4\pi r'p'(r')\right)^2\right) = 0, \end{aligned} \quad (\text{A.12})$$

$$\begin{aligned} \frac{d^2 \tilde{H}_l(r')}{dr'^2 x^2 M_{pl}^2} - \frac{d\tilde{H}_l(r')}{dr' x^2 M_{pl}^2} \left(1 - 2\frac{m'(r')}{r'}\right)^{-1} 4\pi r'(\rho'(r') + p'(r')) \\ - \frac{\tilde{H}_l(r')}{x^2 M_{pl}^2} \left(1 - 2\frac{m'(r')}{r'}\right)^{-1} \left(\frac{l(l+1)}{r'^2} - \frac{4m'(r')}{r'^3} + 8\pi\theta(p'(r') + \rho'(r'))\right) = 0. \end{aligned} \quad (\text{A.13})$$

Thus, if we define $H'_l = H_l/x^2 M_{pl}^2$ and $\tilde{H}'_l = \tilde{H}_l/x^2 M_{pl}^2$, the equations become completely free of x , as we know from self-similar TOV that $m'(r)$, $p'(r)$, $\epsilon'(r)$ are completely independent of x and only depend on the central density. Thus, $H'_l(r')$ and $\tilde{H}'_l(r')$ are independent of x . This also means that $y'_l(R')$ and $\tilde{y}'_l(R')$ are independent of x . We can use these functions to calculate y_l and \tilde{y}_l for arbitrary EoS using

$$y_l(R) = \frac{R}{H_l(R)} \frac{dH_l(R)}{dR} = \frac{R'}{H'_l(R')} \frac{dH'_l(R')}{dR'} = y'_l(R' = R/xM_{pl}), \quad (\text{A.14})$$

$$\tilde{y}_l(R) = \frac{R}{\tilde{H}_l(R)} \frac{d\tilde{H}_l(R)}{dR} = \frac{R'}{\tilde{H}'_l(R')} \frac{d\tilde{H}'_l(R')}{dR'} = \tilde{y}'_l(R' = R/xM_{pl}) \quad (\text{A.15})$$

Thus, for a fixed $M'/R'/C$, the y_l , \tilde{y}_l and consequently k_l , j_l , Λ_l and Σ_l are fixed and do not depend on x . $\Lambda_l(M')$ and $\Sigma(M')$ are thus EoS independent and can be used to obtain the

corresponding quantities for arbitrary EoS using mass scaling. For example, the quadrupolar dimensionless tidal deformability of arbitrary EoS (parametrized by x) and mass configuration can be obtained as $\Lambda_2(x, M) = \Lambda_2(M' = M/xM_{Pl}^3)$. We have shown this for tidal Love numbers and dimensionless tidal deformability of all orders and both types.

B Variation with density

We perform another preliminary check in Fig. 14(a). We plot the mass (M), radius (R), and compactness (C) normalized to their respective maximum values reached for massive BSs as a function of scaled central density. Since the quantities are normalized, these curves are the same for BSs, as, for example, in the case of $M/M_{max} = M'/M'_{max} = M'/0.06$. $R'_{max} = 0.626$ and $C_{max} = 0.16$. Both mass and compactness increase with central density and asymptotically reach zero for low central densities. From the mass curve, we observe that beyond the critical central density $\rho'_c = 1.6$, $\partial M/\partial \rho_c$ becomes negative. Note that the maximum central density reached in a stable BS is $\mathcal{O}(1)$. Thus, the ultra-relativistic limit, where $\rho'_c \gg 1$, $P' = \rho'/3$ is not reached. The compactness reaches a maximum beyond this density, but this is the region where BSs are unstable. Thus, the compactness at this critical density is the maximum compactness reached by stable BSs. We conclude that the maximum central density that can sustain stable configurations of BSs is given by $\rho_c = 1.6/x^2$ for a given (λ, m) . Both mass and compactness undergo oscillations after having reached their maximum. Radius, on the other hand, starts from 1. This means that BSs reach a fixed maximum radius for low central densities. As the density increases, the radius reduces and reaches a minimum at a density beyond the critical density, which then oscillates. The radius at critical density is the minimum radius observed for a stable BS. This corresponds to $R' = 0.38$.

C $\Lambda - M$

In Fig 14(b), we plot the dimensionless tidal deformability Λ as a function of scaled mass. It has been shown the Λ does not scale with x in Appendix. A. Thus, we get a unique $\Lambda - M'$ curve. Λ decreases with mass, and we obtain a minimum value of $\Lambda_{min} = 280$. We also show a fit given in Eq.9 of [56] This can be used to comment on the tidal deformability of BS with any model parameters. Cipriani et al. [21] mention in their work that for a given x , there is a range of masses for which the tidal deformability is measurable. This $\Lambda - M$ relation, along with scaling relations, can be used to get an analytical expression for the same. Vaglio et al. [55] also reported a fit in the form $\Lambda = \Lambda(M')$ (see. Eqs. 11-12 from [55]). These fits are shown in Fig 14(b) for comparison.

For the $l = 2$ tidal love number k_2 , we obtain a minimum value of 0.045 for the highest compactness configuration, and k_2 approaches 0.25 for low compactness. This range is consistent with [56]. For low compactness, the central density for BSs is $\rho'_c \ll 1 \implies P' = \rho'^2/4$. Thus, it follows the polytrope relation $P = K\rho^2$. This is consistent with k_2 for a polytropic EoS $P = K\rho^2$ evaluated in the Newtonian limit, given by $k_2 = \frac{15-\pi^2}{2\pi^2} \approx 0.26$ [99]. We plot k_2 as a function of scaled mass in Fig 14(c) We point out that our result does not match with k_2 evaluated in [56] (shown by blue curve in Fig 14(c)) as they used the fitting function between C and M given by

$$C^{-1} \approx 7.5 + 48.8 \left(1 - \frac{M'}{0.06}\right)^2 \quad (\text{C.1})$$

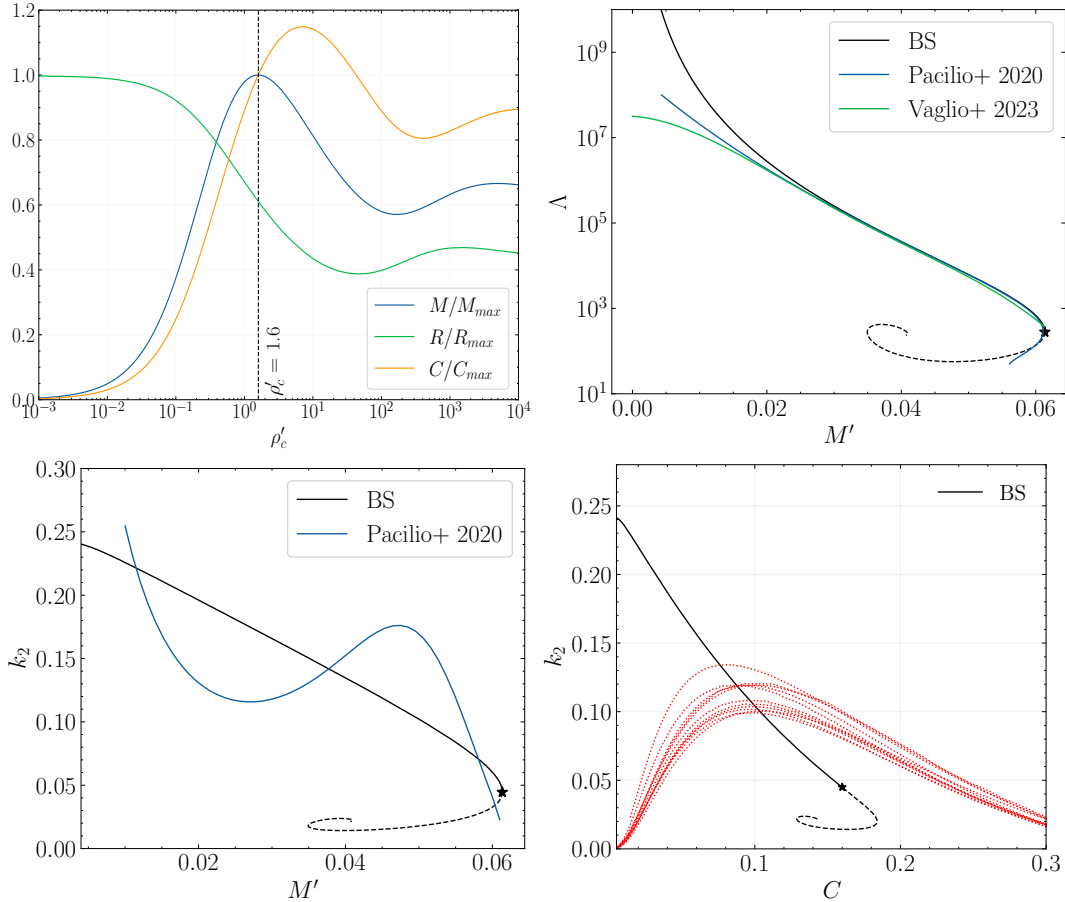


Figure 14. (a) The mass, radius, and compactness normalized by their maximum values as a function of dimensionless central energy density. The vertical dashed line denotes the maximum central density beyond which the star becomes unstable, i.e., $\partial M/\partial \rho_c < 0$. This critical value is $\rho'_c = 1.6$. (b) Dimensionless tidal deformability as a function of scaled mass. The blue and green curves denote the first as provided in [56] and [55], respectively (c) k_2 as a function of scaled mass. The blue curve is derived from $k_2 = 3/2\Lambda C^5$ using the fitting function C.1 as done in [56]. (d) Tidal love number k_2 as a function of C . The red curves are for a few NS EoSs as obtained from the CompOSE database [98]. The star in (b), (c), and (d) marks the point beyond which the BS configurations become unstable, as shown by the dashed curve.

to evaluate k_2 as a function of mass from the relation $k_2 = \Lambda C^5$. As we showed in Fig. 2(a), this $C(M)$ relation is not a good fit for BSs. Moreover, a factor of $3/2$ was missing in the expression for k_2 ($k_2 = \frac{3}{2}\Lambda C^5$), which we have accounted for in the comparison. This is why Fig. 6 of [56] is inconsistent with our results and that from [21]. Also, the tidal love number k_2 as a function of compactness is shown in Fig. 14(d). We show the relation for NSs in red using a few NS EoSs taken from CompOSE [98] for comparison.

D Scaling for Moment of Inertia

The moment of inertia is defined as [100]

$$I \equiv \frac{S}{\Omega}, \quad (\text{D.1})$$

where S and Ω are the angular momentum and the angular spin frequency of the star, BS in our case. This is related to the metric function ω_1 outside the star as

$$\omega_1^{ext} = \Omega - \frac{2S}{R^3} = \Omega \left(1 - \frac{2I}{R^3} \right). \quad (\text{D.2})$$

ω_1 is the metric function (t, ϕ) component of the metric in the Boyer-Lindquist-type coordinates [100]. We define the scaling $I = I' x^3 M_{pl}^3$. Thus, Ω and ω_1 remain invariant under this transformation. The complete expression for the moment of inertia used for computation is given by

$$I = \frac{8\pi}{3} \frac{1}{\Omega} \int_0^R \frac{e^{-(\nu+\lambda)/2} R^5 G(\rho+p) \omega_1}{R - 2GM(R)} dR, \quad (\text{D.3})$$

$$\implies I = \frac{8\pi}{3} \frac{1}{\Omega'} \int_0^{R'} \frac{e^{-(\nu'+\lambda')/2} R'^5 (\rho'+p') \omega_1'(x^3 M_{pl}^3)}{R' - 2M'(R')} dR' \quad (\text{D.4})$$

Using $I = I' x^3 M_{pl}^3$, the equations become independent of x . The dimensionless moment of inertia (\bar{I}) is defined as

$$\bar{I} \equiv \frac{I}{(GM)^3} = \frac{I'}{M'^3} = \bar{I}'. \quad (\text{D.5})$$

Thus, the dimensionless moment of inertia does not scale with model parameters.

E The I –Love– C Relations

The I -Love- Q universal relations connecting the moment of inertia, the tidal deformability, and the spin-induced quadrupole moments for NSs have been known for a long time [100]. This means that they are followed regardless of the underlying EoS. These relations were shown to be followed by dark BSs by Maselli et al. [41] for select values of $\lambda \in 0.5, 1.0, 1.5\pi$ and $m \in 300, 400$ MeV. These are shown in the orange patch in Fig. 1. They found that the dark BSs with these model parameters admit the I -Love- Q universal relations, i.e., all BS EoSs followed it regardless of the model parameters. This was confirmed by another recent work for a few BS models [87]. This was an empirical observation. Here, we prove theoretically that BSs follow these universal relations.

We focus on the I -Love relations here and their dependence on compactness. We do not consider the spin-induced quadrupole moments as we restrict them to non-spinning BSs. Also, spinning scalar BSs are known to lose sphericity from torus/donut-shaped configurations [35]. Note that in this relation, the dimensionless moment of inertia ($\bar{I} = I/M^3$) is related to the dimensionless tidal deformability (Λ). In Appendix A and Appendix D we explicitly show that Λ and \bar{I} are independent of model parameters (λ, m). Thus, we can obtain the $\bar{I} - \Lambda$ curve for any EoS for BS, and this is followed by all the EoSs. This is also the reason why all the curves I -Love- Q obtained for different EoS parameters in [41] exactly overlap without having any spread.

We show this $\bar{I} - \Lambda$ in Fig.15(a). The black dashed curve is the numerical solution obtained for the scaled EoS. We further plot the relation obtained for NSs by [100] for the sake of comparison in green. We conclude there is a degeneracy with NSs, and this relation does not break it. The blue curve shows the I -Love fit as obtained in [41] for BSs. The fit coefficients are given in Table. 4 with $X = \log \Lambda$, and $Y = \log \bar{I}$. This is in excellent agreement with our results as it fits within an accuracy of 1%, thus providing a check of veracity for our

Y	X	b_0	b_1	b_2	b_3	b_4
$\log \bar{I}$	$\log \Lambda$	1.38	9.46×10^{-2}	1.84×10^{-2}	-5.84×10^{-4}	5.51×10^{-6}
C	$\log \Lambda$	2.859×10^{-1}	-2.068×10^{-2}	-8.276×10^{-4}	1.139×10^{-4}	-2.781×10^{-6}
\bar{I}	$1/C$	–	1.532×10^{-1}	2.664×10^{-1}	-1.317×10^{-4}	1.535×10^{-6}

Table 4. Fitting coefficients for the fits between the quantities \bar{I} , Λ' , and C' for massive BSs in strong-interaction limit. The fitting function is given in Eqs. 4.1. The coefficients for the I -Love relation are the same as they were reported in [41].

results. However, the same fit had an error of about 10% in [41] (see Fig. 7 of [41]). Thus, we find the fit to be better than what was claimed before and do not provide any new relation here. [41] also find a universal relation for $k_2 - C$. Note that [87] also reported a similar fit relation using select BS models. In Appendix. A, we have proved the same, i.e., we have shown that k_2 is also EoS independent, i.e., they do not scale with x .

We also show the C -Love and \bar{I} - C relations in Figs. 15(b) and 15(c), respectively. We did not find these relations in the literature for BSs. Both of these are decreasing functions. We use the same functional forms for BSs as used in [101] for NSs and quark stars (QSs). For the C -Love relation we use

$$C = \sum_{k=0}^4 b_k (\ln \Lambda)^k, \quad (\text{E.1})$$

while for the \bar{I} - C relation we use

$$\bar{I} = \sum_{k=1}^4 b_k C^{-k}. \quad (\text{E.2})$$

These are all in the form Eq. 4.1. The fit coefficients for all the cases are given in Table. 4. The corresponding relations for NSs reported in [101] are shown in blue dashed curves. We plot it in only those regimes for which they were derived, i.e., for $C \geq 0.1$ and $\Lambda \leq 10^4$. We find that both the relations diverge with higher compactness (or higher mass, or lower Λ).

In the case of NSs, the relations involving compactness have an uncertainty of up to 10% owing to the uncertainty in EoS [101], while the I -Love relation is much more accurate with an error under 1% [101]. In the case of BS, however, we claim that all these relations are exact, i.e., the relation does not depend at all on the model parameters (or equivalently on x). All the fits have an error below 2%.

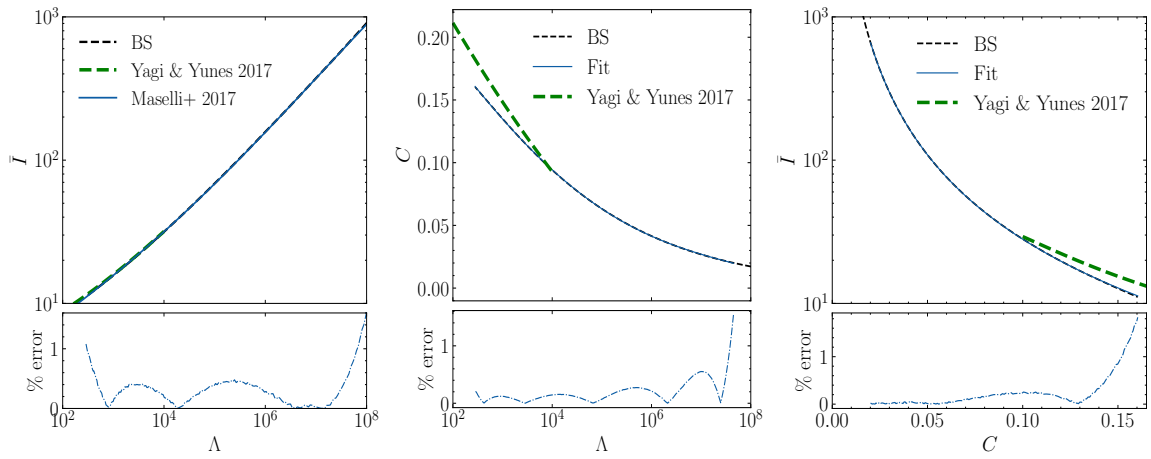


Figure 15. The (a) \bar{I} -Love (b) C -Love and (c) \bar{I} - C relations for massive BSs in the strong-interaction limit. The blue curve in (a) is the fit provided in [41]. For the other two relations, we provide the fits we performed as discussed in the text. The I -Love- C fits as provided in [101] for NSs are shown in green. We have shown this up to $C = 0.1$ ($\Lambda = 10^4$) as appropriate for NSs. The errors corresponding to the fits are shown in the lower panels in each case.

References

- [1] L. Visinelli, *Boson stars and oscillatons: A review*, *International Journal of Modern Physics D* **30** (2021) 2130006 [2109.05481].
- [2] S.L. Liebling and C. Palenzuela, *Dynamical boson stars*, *Living Reviews in Relativity* **26** (2023) 1.
- [3] P. Ralegankar, D. Perri and T. Kobayashi, *Gravothermalizing into primordial black holes, boson stars, and cannibal stars*, *arXiv e-prints* (2024) arXiv:2410.18948 [2410.18948].
- [4] E. Seidel and W.-M. Suen, *Formation of solitonic stars through gravitational cooling*, *Physical Review Letters* **72** (1994) 2516 [gr-qc/9309015].
- [5] V. Cardoso and P. Pani, *Testing the nature of dark compact objects: a status report*, *Living Reviews in Relativity* **22** (2019) 4 [1904.05363].
- [6] P. Jetzer, *Boson stars*, *Physics Reports* **220** (1992) 163.
- [7] J.A. Wheeler, *Geons*, *Physical Review* **97** (1955) 511.
- [8] D.A. Feinblum and W.A. McKinley, *Stable States of a Scalar Particle in Its Own Gravitational Field*, *Physical Review* **168** (1968) 1445.
- [9] D.J. Kaup, *Klein-Gordon Geon*, *Physical Review* **172** (1968) 1331.
- [10] R. Ruffini and S. Bonazzola, *Systems of Self-Gravitating Particles in General Relativity and the Concept of an Equation of State*, *Physical Review* **187** (1969) 1767.
- [11] E.W. Mielke and R. Scherzer, *Geon-type solutions of the nonlinear Heisenberg-Klein-Gordon equation*, *Physical Review D* **24** (1981) 2111.
- [12] M. Colpi, S.L. Shapiro and I. Wasserman, *Boson stars: Gravitational equilibria of self-interacting scalar fields*, *Physical Review Letters* **57** (1986) 2485.
- [13] H. Olivares, Z. Younsi, C.M. Fromm, M. De Laurentis, O. Porth, Y. Mizuno et al., *How to tell an accreting boson star from a black hole*, *Monthly Notices of the Royal Astronomical Society* **497** (2020) 521 [1809.08682].
- [14] J.L. Rosa, J. Pelle and D. Pérez, *Accretion disks and relativistic line broadening in boson star spacetimes*, *Physical Review D* **110** (2024) 084068 [2403.11540].
- [15] B.P. Abbott, R. Abbott, T.D. Abbott, M.R. Abernathy, F. Acernese, K. Ackley et al., *Observation of Gravitational Waves from a Binary Black Hole Merger*, *Physical Review Letters* **116** (2016) 061102 [1602.03837].
- [16] C. Palenzuela, I. Olabarrieta, L. Lehner and S.L. Liebling, *Head-on collisions of boson stars*, *Physical Review D* **75** (2007) 064005 [gr-qc/0612067].
- [17] C. Palenzuela, L. Lehner and S.L. Liebling, *Orbital dynamics of binary boson star systems*, *Physical Review D* **77** (2008) 044036 [0706.2435].
- [18] V. Cardoso, S. Hopper, C.F.B. Macedo, C. Palenzuela and P. Pani, *Gravitational-wave signatures of exotic compact objects and of quantum corrections at the horizon scale*, *Physical Review D* **94** (2016) 084031 [1608.08637].
- [19] C. Palenzuela, P. Pani, M. Bezares, V. Cardoso, L. Lehner and S. Liebling, *Gravitational wave signatures of highly compact boson star binaries*, *Physical Review D* **96** (2017) 104058 [1710.09432].
- [20] A. Urbano and H. Veermäe, *On gravitational echoes from ultracompact exotic stars*, *Journal of Cosmology and Astroparticle Physics* **2019** (2019) 011 [1810.07137].
- [21] L. Cipriani, M. Mannarelli, F. Nesti and S. Trabucco, *Superfluid dark stars*, *arXiv e-prints* (2024) arXiv:2403.03833 [2403.03833].

- [22] T. Evstafyeva, U. Sperhake, I.M. Romero-Shaw and M. Agathos, *Gravitational-Wave Data Analysis with High-Precision Numerical Relativity Simulations of Boson Star Mergers*, *Physical Review Letters* **133** (2024) 131401 [2406.02715].
- [23] R. Abbott, T.D. Abbott, S. Abraham, F. Acernese, K. Ackley, C. Adams et al., *GW190521: A Binary Black Hole Merger with a Total Mass of $150 M_{\odot}$* , *Physical Review Letters* **125** (2020) 101102 [2009.01075].
- [24] J. Sakstein, D. Croon, S.D. McDermott, M.C. Straight and E.J. Baxter, *Beyond the Standard Model Explanations of GW190521*, *Physical Review Letters* **125** (2020) 261105 [2009.01213].
- [25] J.C. Bustillo, N. Sanchis-Gual, A. Torres-Forné, J.A. Font, A. Vajpeyi, R. Smith et al., *GW190521 as a Merger of Proca Stars: A Potential New Vector Boson of 8.7×10^{-13} eV*, *Physical Review Letters* **126** (2021) 081101 [2009.05376].
- [26] C.D. Capano, M. Cabero, J. Westerweck, J. Abedi, S. Kastha, A.H. Nitz et al., *Multimode Quasinormal Spectrum from a Perturbed Black Hole*, *Physical Review Letters* **131** (2023) 221402 [2105.05238].
- [27] Y. Kojima, S. Yoshida and T. Futamase, *Non-Radial Pulsation of a Boson Star. I —Formulation—*, *Progress of Theoretical Physics* **86** (1991) 401.
- [28] S. Yoshida, Y. Eriguchi and T. Futamase, *Quasinormal modes of boson stars*, *Physical Review D* **50** (1994) 6235.
- [29] J. Balakrishna, E. Seidel and W.-M. Suen, *Dynamical evolution of boson stars. II. Excited states and self-interacting fields*, *Physical Review D* **58** (1998) 104004 [gr-qc/9712064].
- [30] C.F.B. Macedo, P. Pani, V. Cardoso and L.C.B. Crispino, *Astrophysical signatures of boson stars: Quasinormal modes and inspiral resonances*, *Physical Review D* **88** (2013) 064046 [1307.4812].
- [31] C. Vásquez Flores, A. Parisi, C.-S. Chen and G. Lugones, *Fundamental oscillation modes of self-interacting bosonic dark stars*, *Journal of Cosmology and Astroparticle Physics* **2019** (2019) 051 [1901.07157].
- [32] B. Kain, *Boson stars and their radial oscillations*, *Physical Review D* **103** (2021) 123003 [2106.01740].
- [33] M. Celato, C.J. Krüger and K.D. Kokkotas, *Probing dark star parameters through f-mode gravitational wave signals*, *Physical Review D* **111** (2025) 023034 [2501.12031].
- [34] S. Shirke, B.K. Pradhan, D. Chatterjee, L. Sagunski and J. Schaffner-Bielich, *Fundamental Oscillations of Massive Boson Stars and Distinguishability*, *arXiv* (2025) .
- [35] N. Sanchis-Gual, F. Di Giovanni, M. Zilhão, C. Herdeiro, P. Cerdá-Durán, J.A. Font et al., *Nonlinear Dynamics of Spinning Bosonic Stars: Formation and Stability*, *Physical Review Letters* **123** (2019) 221101 [1907.12565].
- [36] P. Amaro-Seoane, J. Barranco, A. Bernal and L. Rezzolla, *Constraining scalar fields with stellar kinematics and collisional dark matter*, *Journal of Cosmology and Astroparticle Physics* **2010** (2010) 002 [1009.0019].
- [37] D. Rafiei Karkevandi, S. Shakeri, V. Sagun and O. Ivanytskyi, *Bosonic dark matter in neutron stars and its effect on gravitational wave signal*, *Physical Review D* **105** (2022) 023001 [2109.03801].
- [38] J. Eby, C. Kouvaris, N.G. Nielsen and L.C.R. Wijewardhana, *Boson stars from self-interacting dark matter*, *Journal of High Energy Physics* **2016** (2016) 28 [1511.04474].
- [39] J.A.R. Cembranos, A.L. Maroto, S.J. Núñez Jareño and H. Villarrubia-Rojo, *Constraints on anharmonic corrections of fuzzy dark matter*, *Journal of High Energy Physics* **2018** (2018) 73 [1805.08112].

- [40] T. Zimmermann, J. Alvey, D.J.E. Marsh, M. Fairbairn and J.I. Read, *Dwarf galaxies imply dark matter is heavier than 2.2×10^{-21} eV*, *arXiv e-prints* (2024) arXiv:2405.20374 [2405.20374].
- [41] A. Maselli, P. Pnigouras, N.G. Nielsen, C. Kouvaris and K.D. Kokkotas, *Dark stars: Gravitational and electromagnetic observables*, *Physical Review D* **96** (2017) 023005 [1704.07286].
- [42] S. Tulin and H.-B. Yu, *Dark matter self-interactions and small scale structure*, *Physics Reports* **730** (2018) 1 [1705.02358].
- [43] Event Horizon Telescope Collaboration, K. Akiyama, A. Alberdi, W. Alef, J.C. Algaba, R. Anantua et al., *First Sagittarius A* Event Horizon Telescope Results. I. The Shadow of the Supermassive Black Hole in the Center of the Milky Way*, *The Astrophysical Journal Letters* **930** (2022) L12.
- [44] Event Horizon Telescope Collaboration, K. Akiyama, A. Alberdi, W. Alef, K. Asada, R. Azulay et al., *First M87 Event Horizon Telescope Results. I. The Shadow of the Supermassive Black Hole*, *The Astrophysical Journal Letters* **875** (2019) L1 [1906.11238].
- [45] A. Arbey, J. Lesgourgues and P. Salati, *Galactic halos of fluid dark matter*, *Physical Review D* **68** (2003) 023511 [astro-ph/0301533].
- [46] M. Dentler, D.J.E. Marsh, R. Hložek, A. Laguë, K.K. Rogers and D. Grin, *Fuzzy dark matter and the Dark Energy Survey Year 1 data*, *Monthly Notices of the Royal Astronomical Society* **515** (2022) 5646 [2111.01199].
- [47] K.K. Rogers and H.V. Peiris, *Strong Bound on Canonical Ultralight Axion Dark Matter from the Lyman-Alpha Forest*, *Physical Review Letters* **126** (2021) 071302 [2007.12705].
- [48] E.O. Nadler, A. Drlica-Wagner, K. Bechtol, S. Mau, R.H. Wechsler, V. Gluscevic et al., *Constraints on Dark Matter Properties from Observations of Milky Way Satellite Galaxies*, *Physical Review Letters* **126** (2021) 091101 [2008.00022].
- [49] H. Winch, K.K. Rogers, R. Hložek and D.J.E. Marsh, *High-redshift, small-scale tests of ultralight axion dark matter using Hubble and Webb galaxy UV luminosities*, *arXiv e-prints* (2024) arXiv:2404.11071 [2404.11071].
- [50] Planck Collaboration, P.A.R. Ade, N. Aghanim, M. Arnaud, M. Ashdown, J. Aumont et al., *Planck 2015 results. XIII. Cosmological parameters*, *Astronomy and Astrophysics* **594** (2016) A13 [1502.01589].
- [51] D. Parkinson, S. Riemer-Sørensen, C. Blake, G.B. Poole, T.M. Davis, S. Brough et al., *The WiggleZ Dark Energy Survey: Final data release and cosmological results*, *Physical Review D* **86** (2012) 103518 [1210.2130].
- [52] Z. Rezaei, *Fuzzy dark matter in relativistic stars*, *Monthly Notices of the Royal Astronomical Society* **524** (2023) 2015 [2306.17665].
- [53] J. Yang, P.V.P. Cunha and C.A.R. Herdeiro, *Analytical proxy to families of numerical solutions: the case study of spherical mini-boson stars*, *Journal of Cosmology and Astroparticle Physics* **2024** (2024) 055 [2405.15651].
- [54] F.D. Ryan, *Spinning boson stars with large self-interaction*, *Physical Review D* **55** (1997) 6081.
- [55] M. Vaglio, C. Pacilio, A. Maselli and P. Pani, *Bayesian parameter estimation on boson-star binary signals with a coherent inspiral template and spin-dependent quadrupolar corrections*, *Physical Review D* **108** (2023) 023021 [2302.13954].
- [56] C. Pacilio, M. Vaglio, A. Maselli and P. Pani, *Gravitational-wave detectors as particle-physics laboratories: Constraining scalar interactions with a coherent inspiral model of boson-star binaries*, *Physical Review D* **102** (2020) 083002 [2007.05264].

- [57] N. Sennett, T. Hinderer, J. Steinhoff, A. Buonanno and S. Ossokine, *Distinguishing boson stars from black holes and neutron stars from tidal interactions in inspiraling binary systems*, *Physical Review D* **96** (2017) 024002 [1704.08651].
- [58] N. Andersson and K.D. Kokkotas, *Gravitational Waves and Pulsating Stars: What Can We Learn from Future Observations?*, *Physical Review Letters* **77** (1996) 4134 [gr-qc/9610035].
- [59] N. Andersson and K.D. Kokkotas, *Towards gravitational wave asteroseismology*, *Monthly Notices of the Royal Astronomical Society* **299** (1998) 1059 [gr-qc/9711088].
- [60] O. Benhar, V. Ferrari and L. Gualtieri, *Gravitational wave asteroseismology reexamined*, *Physical Review D* **70** (2004) 124015 [astro-ph/0407529].
- [61] B.K. Pradhan, D. Chatterjee, M. Lanoye and P. Jaikumar, *General relativistic treatment of f -mode oscillations of hyperonic stars*, *Physical Review C* **106** (2022) 015805.
- [62] S. Shirke, S. Ghosh, D. Chatterjee, L. Sagunski and J. Schaffner-Bielich, *R-modes as a New Probe of Dark Matter in Neutron Stars*, *arXiv e-prints* (2023) arXiv:2305.05664 [2305.05664].
- [63] T.K. Chan, Y.H. Sham, P.T. Leung and L.M. Lin, *Multipolar universal relations between f -mode frequency and tidal deformability of compact stars*, *Physical Review D* **90** (2014) 124023 [1408.3789].
- [64] H. Sotani and B. Kumar, *Universal relations between the quasinormal modes of neutron star and tidal deformability*, *Physical Review D* **104** (2021) 123002.
- [65] B.K. Pradhan, A. Vijaykumar and D. Chatterjee, *Impact of updated multipole Love numbers and f -Love universal relations in the context of binary neutron stars*, *Physical Review D* **107** (2023) 023010 [2210.09425].
- [66] S. Kawamura, M. Ando, N. Seto, S. Sato, T. Nakamura, K. Tsubono et al., *The Japanese space gravitational wave antenna: DECIGO*, *Classical and Quantum Gravity* **28** (2011) 094011.
- [67] K.A. Kuns, H. Yu, Y. Chen and R.X. Adhikari, *Astrophysics and cosmology with a decihertz gravitational-wave detector: TianGO*, *Physical Review D* **102** (2020) 043001 [1908.06004].
- [68] W.C.G. Ho, D.I. Jones, N. Andersson and C.M. Espinoza, *Gravitational waves from transient neutron star f -mode oscillations*, *Physical Review D* **101** (2020) 103009 [2003.12082].
- [69] B.K. Pradhan, D. Pathak and D. Chatterjee, *Constraining Nuclear Parameters Using Gravitational Waves from f -mode Oscillations in Neutron Stars*, *The Astrophysical Journal* **956** (2023) 38 [2306.04626].
- [70] F. Echeverria, *Gravitational-wave measurements of the mass and angular momentum of a black hole*, *Physical Review D* **40** (1989) 3194.
- [71] K.D. Kokkotas, T.A. Apostolatos and N. Andersson, *The inverse problem for pulsating neutron stars: a ‘fingerprint analysis’ for the supranuclear equation of state*, *Monthly Notices of the Royal Astronomical Society* **320** (2001) 307 [gr-qc/9901072].
- [72] T. Robson, N.J. Cornish and C. Liu, *The construction and use of LISA sensitivity curves*, *Classical and Quantum Gravity* **36** (2019) 105011 [1803.01944].
- [73] L.K. Tsui and P.T. Leung, *Universality in quasi-normal modes of neutron stars*, *Monthly Notices of the Royal Astronomical Society* **357** (2005) 1029 [https://academic.oup.com/mnras/article-pdf/357/3/1029/18164114/357-3-1029.pdf].
- [74] D.D. Doneva, E. Gaertig, K.D. Kokkotas and C. Krüger, *Gravitational wave asteroseismology of fast rotating neutron stars with realistic equations of state*, *Physical Review D* **88** (2013) 044052 [1305.7197].
- [75] B.K. Pradhan and D. Chatterjee, *Effect of hyperons on f -mode oscillations in neutron stars*, *Physical Review C* **103** (2021) 035810 [2011.02204].

- [76] I.A. Rather, K.D. Marquez, P. Thakur and O. Lourenço, *Non-radial oscillation modes in hybrid stars with hyperons and delta baryons: Full general relativity formalism vs. cowling approximation*, 2024.
- [77] H. Sotani, N. Yasutake, T. Maruyama and T. Tatsumi, *Signatures of hadron-quark mixed phase in gravitational waves*, *Physical Review D* **83** (2011) 024014 [[1012.4042](#)].
- [78] T. Zhao and J.M. Lattimer, *Universal relations for neutron star f -mode and g -mode oscillations*, *Physical Review D* **106** (2022) 123002 [[2204.03037](#)].
- [79] H. Sotani and T. Kojo, *Universality in quasinormal modes of neutron stars with quark-hadron crossover*, *Physical Review D* **108** (2023) 063004 [[2308.11494](#)].
- [80] I.F. Ranea-Sandoval, M. Mariani, M.O. Celi, M.C. Rodríguez and L. Tonetto, *Asteroseismology using quadrupolar f -modes revisited: Breaking of universal relationships in the slow hadron-quark conversion scenario*, *Physical Review D* **107** (2023) 123028 [[2306.02823](#)].
- [81] B.K. Pradhan, D. Chatterjee and D.E. Alvarez-Castillo, *Probing hadron-quark phase transition in twin stars using f -modes*, *Monthly Notices of the Royal Astronomical Society* **531** (2024) 4640 [[2309.08775](#)].
- [82] H.C. Das, A. Kumar, S.K. Biswal and S.K. Patra, *Impacts of dark matter on the f -mode oscillation of hyperon star*, *Physical Review D* **104** (2021) 123006.
- [83] C.V. Flores, C.H. Lenzi, M. Dutra, O. Lourenço and J.D.V. Arbañil, *Gravitational wave asteroseismology of dark matter hadronic stars*, *Physical Review D* **109** (2024) 083021 [[2402.12600](#)].
- [84] S. Shirke, B.K. Pradhan, D. Chatterjee, L. Sagunski and J. Schaffner-Bielich, *Effects of dark matter on f -mode oscillations of neutron stars*, *Physical Review D* **110** (2024) 063025 [[2403.18740](#)].
- [85] P. Thakur, T. Malik, A. Das, T.K. Jha, B.K. Sharma and C. Providência, *Feasibility of dark matter admixed neutron star based on recent observational constraints*, *arXiv e-prints* (2024) [arXiv:2408.03780](#) [[2408.03780](#)].
- [86] D. Dey, J. Amrit Pattnaik, R.N. Panda, M. Bhuyan and S.K. Patra, *f -mode oscillations of dark matter admixed quarkyonic neutron star*, *arXiv e-prints* (2024) [arXiv:2412.06739](#) [[2412.06739](#)].
- [87] J.-Y. Wu, W. Li, X.-H. Huang and K. Zhang, *Dark I-Love-Q*, *arXiv e-prints* (2023) [arXiv:2309.07971](#) [[2309.07971](#)].
- [88] V. Cardoso, E. Franzin, A. Maselli, P. Pani and G. Raposo, *Testing strong-field gravity with tidal Love numbers*, *Physical Review D* **95** (2017) 084014 [[1701.01116](#)].
- [89] G.F. Giudice, M. McCullough and A. Urbano, *Hunting for dark particles with gravitational waves*, *Journal of Cosmology and Astroparticle Physics* **2016** (2016) 001 [[1605.01209](#)].
- [90] M. Bezares and C. Palenzuela, *Gravitational waves from dark boson star binary mergers*, *Classical and Quantum Gravity* **35** (2018) 234002 [[1808.10732](#)].
- [91] D. Croon, J. Fan and C. Sun, *Boson star from repulsive light scalars and gravitational waves*, *Journal of Cosmology and Astroparticle Physics* **2019** (2019) 008 [[1810.01420](#)].
- [92] H.-K. Guo, K. Sinha and C. Sun, *Probing boson stars with extreme mass ratio inspirals*, *Journal of Cosmology and Astroparticle Physics* **2019** (2019) 032 [[1904.07871](#)].
- [93] S.L. Pitz and J. Schaffner-Bielich, *Generating ultracompact boson stars with modified scalar potentials*, *Physical Review D* **108** (2023) 103043 [[2308.01254](#)].

- [94] E. Barausse, R. Brito, V. Cardoso, I. Dvorkin and P. Pani, *The stochastic gravitational-wave background in the absence of horizons*, *Classical and Quantum Gravity* **35** (2018) 20LT01 [1805.08229].
- [95] D. Croon, M. Gleiser, S. Mohapatra and C. Sun, *Gravitational radiation background from boson star binaries*, *Physics Letters B* **783** (2018) 158 [1802.08259].
- [96] H. Banks, D.M. Grabowska and M. McCullough, *Gravitational wave backgrounds from colliding exotic compact objects*, *Physical Review D* **108** (2023) 035017 [2302.07887].
- [97] L. Perot and N. Chamel, *Role of dense matter in tidal deformations of inspiralling neutron stars and in gravitational waveforms with unified equations of state*, *Physical Review C* **103** (2021) 025801 [2102.02004].
- [98] “Compose database.” <https://compose.obspm.fr/>.
- [99] S. Postnikov, M. Prakash and J.M. Lattimer, *Tidal Love numbers of neutron and self-bound quark stars*, *Physical Review D* **82** (2010) 024016 [1004.5098].
- [100] K. Yagi and N. Yunes, *I-Love-Q relations in neutron stars and their applications to astrophysics, gravitational waves, and fundamental physics*, *Physical Review D* **88** (2013) 023009 [1303.1528].
- [101] K. Yagi and N. Yunes, *Approximate universal relations for neutron stars and quark stars*, *Physics Reports* **681** (2017) 1 [1608.02582].